ISSN 1541-308X, Physics of Wave Phenomena, 2022, Vol. 30, No. 4, pp. 217–241. © Allerton Press, Inc., 2022.

MESOSCOPIC OPTICS

Optical Phenomena in Dielectric Spheres Several Light Wavelengths in Size: A Review

B. S. Luk'yanchuk[a, *], A. R. Bekirov[a], Z. B. Wang[b], I. V. Minin[c, d], O. V. Minin[c,d], and A. A. Fedyanin[a]

[a] *Faculty of Physics, Lomonosov Moscow State University, Moscow, 119991 Russia*

[b] *School of Computer Science and Electronic Engineering, Bangor University, Bangor, LL57 1UT, UK*

[c] *Tomsk Polytechnical University, Tomsk, 634050 Russia*

[d] *Siberian State University of Geosystems and Technologies, Novosibirsk, 630108 Russia*

**e-mail: lukiyanchuk@nanolab.phys.msu.ru*

Received February 10, 2022; revised March 24, 2022; accepted April 11, 2022

Abstract—The size parameter $q = 2\pi R/\lambda$ in spheres with a radius $R = (2–3)\lambda$ (λ is the radiation wavelength) is on the order of 10. Strong Mie resonances ($\ell \geq 5$) are observed in these structures; these resonances lead to peculiar optical phenomena, caused by the interference of high-order multipoles and localization of magnetic fields. Examples of such optical phenomena are presented in this review.

Keywords: spherical particle, mesoscale, Mie theory, photonic nanojet, magnetic light, Fano resonances, anapole, giant magnetic fields

DOI: 10.3103/S1541308X22040045

1. INTRODUCTION

In 1908 G. Mie published the study *Beiträge zur Optik trüber Medien, speziell kolloidaler Metallösungen* [1], which was devoted to the analytical solution of Maxwell's equations for a homogeneous spherical particle irradiated by a plane electromagnetic wave. Mie was not the first theoretician who found a correct solution to this problem. The corresponding formulas had been derived previously by some other researchers [2]. Incidentally, Mie referred to the Lorenz study in [1], and the Mie theory is sometimes called the Lorenz–Mie theory. Mie's merit is that he was the first to draw attention to the following fact: the color of colloidal solutions is determined by the phenomena of resonant light scattering from nanoparticles with a complex refractive index. This is a fundamental difference of Mie scattering from nonresonant Rayleigh scattering for the case where the particle size is much smaller than the radiation wavelength. Naturally, Rayleigh scattering is a particular case of Mie scattering. In essence, Mie was the first to analyze theoretically the formation of localized plasmons. Mie's study was of moderate interest during the next 70 years; however, since the beginning of the 1990s, an avalanche-like rise in the number of publications concerning the "Mie theory" was observed (Fig. 1). The intensity of publications correlates with the intensity of publications in the field of plasmonics [3, 4]; it is also related to the discovery of new optical phenomena occurring upon light scattering from structures several wavelengths in size. It turned out that new physical effects were encoded in the formulas of the Mie theory, and they were just waiting for somebody to decipher them. Figure 1 presents quotations from several recent publications, concerning the physical effects related to the discovery of photonic nanojet, Fano resonances in plasmonics, and optical anapole. The calculation of fields within the Mie theory is a rather time-consuming task, but it was not the software that led to progress in optics. The "insight" into some optical phenomena was related to "the second degree of understanding," as defined by L.I. Mandelstam, i.e., with a change in the point of view for the known formulas.

The formulas of the Mie theory present expansions of fields in spherical harmonics. The expansion coefficients satisfy boundary conditions: continuity of field tangential components on the sphere surface. The scattering efficiency (scattering cross section normalized to the geometric cross section: $Q_{sca} = \sigma_{sca}/\pi R^2$, where R is the spherical particle radius) is expressed in the simplest way in the Mie theory. This value is presented as the sum of multipole—dipole ($\ell = 1$), quadrupole ($\ell = 2$), octupole ($\ell = 3$), etc.—amplitudes:

$$Q_{sca} = \sum_{\ell=1}^{\infty}\left(Q_\ell^{(e)} + Q_\ell^{(m)}\right), \quad Q_\ell^{(e)} = \frac{2(2\ell+1)}{q_m^2}|a_\ell|^2, \quad Q_\ell^{(m)} = \frac{2(2\ell+1)}{q_m^2}|b_\ell|^2. \tag{1}$$

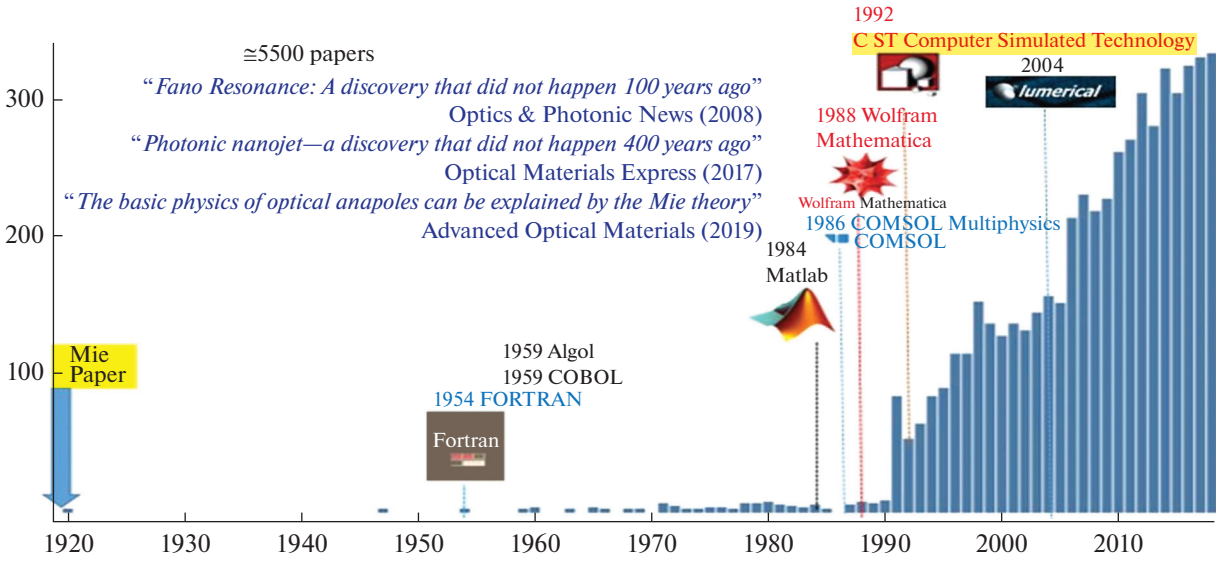

Fig. 1. (Color online) Number of publications devoted to the Mie theory, according to the Web of Science [5].

Here, $Q_\ell^{(e)}$ and $Q_\ell^{(m)}$ are the partial efficiencies, associated with the ℓth-order multipole moments. The electric, a_ℓ, and magnetic, b_ℓ, scattering amplitudes are given by the formulas

$$a_\ell = \frac{\Re_\ell^{(a)}}{\Re_\ell^{(a)} + i\Im_\ell^{(a)}}, \quad b_\ell = \frac{\Re_\ell^{(b)}}{\Re_\ell^{(b)} + i\Im_\ell^{(b)}}. \tag{2}$$

where, in the case of nonmagnetic media,

$$\begin{aligned}
\Re_\ell^{(a)} &= n_\mathrm{p}\psi_\ell(q_\mathrm{p})\psi_\ell'(q_\mathrm{m}) - n_\mathrm{m}\psi_\ell(q_\mathrm{m})\psi_\ell'(q_\mathrm{p}),\\
\Im_\ell^{(a)} &= n_\mathrm{p}\psi_\ell(q_\mathrm{p})\chi_\ell'(q_\mathrm{m}) - n_\mathrm{m}\chi_\ell(q_\mathrm{m})\psi_\ell'(q_\mathrm{p}),\\
\Re_\ell^{(b)} &= n_\mathrm{p}\psi_\ell(q_m)\psi_\ell'(q_\mathrm{p}) - n_\mathrm{m}\psi_\ell(q_p)\psi_\ell'(q_\mathrm{m}),\\
\Im_\ell^{(b)} &= n_\mathrm{p}\psi_\ell'(q_\mathrm{p})\chi_\ell(q_\mathrm{m}) - n_\mathrm{m}\chi_\ell'(q_\mathrm{m})\psi_\ell(q_\mathrm{p}).
\end{aligned} \tag{3}$$

Here, the functions $\psi_\ell(z) = \sqrt{\pi z/2}\,J_{\ell+1/2}(z)$ and $\chi_\ell(z) = \sqrt{\pi z/2}\,N_{\ell+1/2}(z)$ are spherical Bessel and Neumann functions [6]. The primes in ψ' and χ' mean differentiation with respect to the corresponding argument, i.e., $\psi_\ell'(z) = d\psi_\ell(z)/dz$. The subscripts m and p in the refractive indices n_m and n_p refer to the external medium and the particle and the values $q_\mathrm{m} = n_\mathrm{m}q$ and $q_\mathrm{p} = n_\mathrm{p}q$, respectively. The value $q = 2\pi R/\lambda$ is the so-called size parameter [6].

According to the Mie theory, the magnetic properties of metal particles in the optical spectral region do not play any significant role in scattering. In the case of dielectric particles, magnetic scattering has a resonant character, and the corresponding electric and magnetic resonances have comparable amplitudes at $n_\mathrm{p} < 2$. The number of multipoles entering formula (1) is determined from the formula $\ell_{\max} = \left|q_\mathrm{m} + 4q_\mathrm{m}^{1/3} + 1\right|$ [7]; therefore, the transition to large particles ($R \gg \lambda$) and geometric optics limit calls for summation of many terms in expression (1) and other formulas of the Mie theory. The principles of geometric optics and the rule for constructing an optical image based on the light refraction law and straight-line propagation of light were formulated by Kepler in 1611. Then this approach was refined based on the eikonal equation [8]. In this case, light scattering from a sphere in the geometric optics limit is reduced to calculation of the Pearcey integral [9–11]. The intensity $I(x, z)$ of scattered light is presented by the squared modulus of function Ψ:

$$\begin{aligned}
I(x,z) &\propto |\Psi|^2,\\
\Psi(x,z) &= \int_{-\infty}^{\infty} \exp\left[-i\left(zt + xt^2 + t^4\right)\right]dt.
\end{aligned} \tag{4}$$

The analysis performed in [11] showed that the approach based on Eq. (4) yields values close to the exact results given by the Mie formulas at size parameters $q_\mathrm{m} > q_{\max}$. The $q_{\max}$ value depends on the refractive index n_p and is determined by comparing the results of calculations in the geometrical optics approximation and within the Mie theory (see Fig. 7 in [11]). One can see in this figure that, at $n_\mathrm{p} = 1.5$ and size parameter values $q = 10$ and 30, the calculation results obtained in the geometrical optics approximation differ significantly from the exact solution, whereas at $q \geq 100$ these results almost coincide. In the formal condition of geometric optics applicability, $q \gg 1$, the "much greater than" sign may indicate in reality "much greater than 10." The characteristic size of these structures significantly exceeds the light wave-

length. In fact, most of classical optics devices, starting with the lenses in the Galileo telescope and Jansen and Leeuwenhoek microscopes, are characterized by very large values of size parameter q in the optical region; therefore, they can be described well by the geometric optics formulas.

Nanotechnologies based on materials with a high refractive index have been actively developed in recent years [12]. Optical elements in these structures are much smaller in size than the light wavelength, and the structures themselves are characterized by size parameters smaller or on the order of unity: $q_m \sim 1$ The optical properties of these structures are generally determined by the first three (dipole, quadrupole, and octupole) Mie resonances, due to which the radiative properties of nanoantennas can be controlled [12–14]. It is of fundamental importance to use wave equations to describe these structures.

Spheres several wavelengths in size, as well as other structures with intermediate values of the size parameter, $q_m \sim 10$, had not been of any special interest for a long time. However, a variety of new optical phenomena (optical nanojets, nanovortices, magnetic light, Fano resonances in dielectric spheres, anapole states and superresolution microscopy, etc.) have been discovered specifically in the range of size parameters: $q_m \approx 5–50$. Our review is devoted to these phenomena, occurring in spheres several light wavelengths in size.

2. PHOTONIC NANOJET AND ITS PRACTICAL APPLICATIONS

It is generally accepted that optics as science originated about three thousand years ago in the period when the first lenses were invented by the ancient Egyptians and Mesopotamians. Actually, the first lenses found by people were water droplets. Even in the period when viticulture arose (five or six thousand years ago), it was known that grapes should not be watered on a sunny afternoon, because small water droplets burn leaves through. Glass manufacturing technology also covers a period of several thousand years. The oldest glass objects—glass balls—date back to the third thousand years B.C., and glass amphorae are found in excavations of the Hellenistic period. An amphora filled with water can play a role of magnifying glass. Pliny the Elder reported on the effect of burning glass in the tenth volume of his Natural History. In essence, a photonic nanojet is a sphere of micrometer size, exhibiting properties of burning glass.

Even though Archimedes, Ptolemy, and most of ancient physicists knew the effect of light refraction, it took about a thousand years to describe theoretically this phenomenon. The corresponding law was correctly formulated for the first time by Ibn Sahl of Baghdad in 984 [15]. Then this law was rediscovered by Thomas Harriot in 1602, Johannes Kepler in 1604, Willebrord Snell in 1621, and René Descartes in 1637 (this law is referred to as the Snell–Descartes law in France). In 1662 Pierre Fermat proved that this law follows from Fermat's principle, according to which light chooses the route characterized by minimum travel time. Finally, in 1678, Christian Huygens demonstrated that Snell's law follows from the wave nature of light and the Huygens–Fresnel principle. According to Arnold's principle [16], "If a notion bears a personal name, then this name is not the name of the discoverer."

In 1609 Galileo invented a two-lens telescope, in which a concave diverging lens formed a virtual, enlarged object image. In 1611 Kepler formulated the rules for constructing an optical image in a telescope based on the refraction law of light and its rectilinear propagation. In essence, Kepler was one of the founders of the geometric optics method. Kepler investigated imaging with thin lenses, but there is doubt that he could analyze in a similar way the focusing effect of a glass ball.

Using ray tracing [18] and Snell's law (the method known since the time of Kepler), one can make sure that the rays refracted on the sphere boundary form a caustic, which is described by the following parametric equation (with all coordinates are normalized to the particle radius):

$$x_c = \left[1 - \frac{1}{2}\frac{\sqrt{n^2 - 1 + \cos^2\varphi} - 2\cos\varphi}{\sqrt{n^2 - 1 + \cos^2\varphi} - \cos\varphi}\cos\varphi\right]\cos\psi, \quad (5)$$
$$y_c = \sec\psi\sin\varphi + x_c\tan\psi,$$

where $\psi = 2\left[\varphi - \arcsin\left(\sin\varphi/n\right)\right]$.

This caustic is presented by a cuspoid curve [18, 19] (Fig. 2). The singularity point is the geometric optics focus (incidentally, the term *focus* was also introduced by Kepler) located at the point

$$x_s = x_c\big|_{\varphi\to 0} = \frac{n}{2(n-1)}. \quad (6)$$

Thus, $x_s \to \infty$ at $n \to 1$, and $x_s \to 1$ at $n \to 2$. At $n > 2$ the caustic is located within the sphere; this holds true for materials with a high refractive index. These materials are used in optically resonant dielectric nanostructures [12], while the substances with a refractive index less than two [17] are the main materials for most of optical components (lenses, optical fibers, etc.). This caustic was analyzed in several studies devoted to the problem of photonic nanojet (see [17] and references therein). Proceeding from Eq. (5) one can determine the numerical aperture $NA = n\sin\chi$, where the angle χ is calculated on the particle surface at $\varphi = \varphi_a = \arccos\sqrt{(n^2-1)/3}$. This estimation yields $NA = n\sqrt{(4-n^2)/3}$. The focus position is determined by the formula

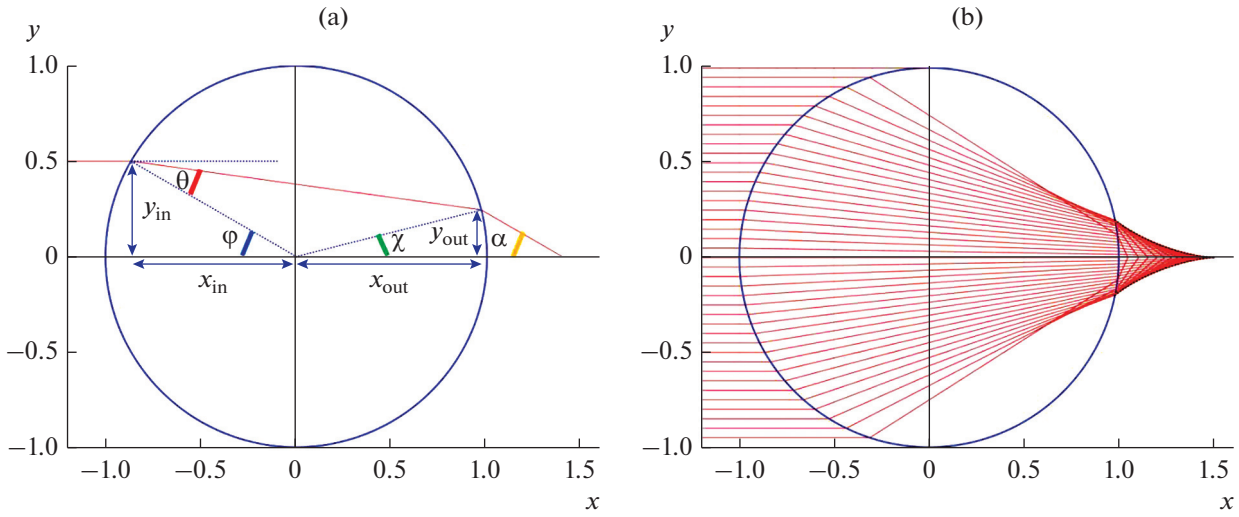

Fig. 2. (Color online) (a) Ray tracing for a large particle with a radius $R \gg \lambda$. The angles of incidence (φ) and refraction (θ) inside the sphere are related by Snell's law: $\sin\varphi = n \sin\theta$. A ray enters the particle at the point with the coordinates $y_{in} = \tan\varphi$ and $x_{in} = -\cos\varphi$. The angles χ and α are given by the formulas $\chi = 2\theta - \varphi$ and $\alpha = 2\varphi - 2\theta$. Two close rays, y_c and y_{cc} (corresponding to the angles φ and $\varphi + \delta\varphi$), at the output of the sphere after the second refraction are intersected at the caustic point $x_c = x_{out} + \partial_\varphi \sin\chi / \partial_\varphi \tan\alpha$, which yields Eq. (5) for the caustic. (b) The shape of caustic from Eq. (5) for a sphere with $n = 1.5$ is shown by a dotted black line (the cuspoid curve, which limits the rays emerging from the sphere) [22].

$$x_f = \frac{2n^6 + 9n^4 + 48n^2 - 32}{6n^2(2+n^2)\sqrt{3(n^2-1)}}. \quad (7)$$

The field intensity at the focus can be estimated as $I = I_0\, 27n^4/(4-n^2)^3$ [20]. Here, I_0 is the incident beam intensity. Within the geometric-optics approach the field intensity at the focus of spherical lens depends on only the lens refractive index and is independent of its size, whereas the focal spot size is proportional to the sphere size and can be much lower than the sphere radius. The light scattering from small particles was investigated by Rayleigh [21]. It followed from the theory that a small dielectric particle with a size $R \ll \lambda$ does not behave as a small lens but scatters light as a point electric dipole (symmetrically in the forward and backward directions). Thus, an asymmetric field distribution arises only in some range of R/λ values, and these values cannot be small. At the same time, according to [11], geometric optics is also applicable for only sufficiently large size parameters. The Mie theory makes it possible to investigate arbitrary n and q values. Some examples are shown in Fig. 3.

It is noteworthy that, under certain conditions, the intensity distribution in the xy cross section, which passes through the photonic jet maximum, overcomes the diffraction limit [22–26]. Due to the possibility of controlling the photonic jet characteristics, this phenomenon can be used in various fields, such as microelectronics [27–30], nanodetection [31], medicine [32, 33], and nanoscopy [34, 35]. The photonic jet effect is used in THz microscopy [36, 37]; it is also applied to increase the sensitivity of receivers 5G and 6G communication devices [38–41]. Among other important applications, we should also mention surface laser cleaning [42]. This phenomenon was discovered independently by several research teams: the group with participation of the Nobel Prize winner A.M. Prokhorov [43] and the IBM European laboratory (priority of patent [44] on 1987). It was shown in the aforementioned studies that, using pulsed laser irradiation, one can remove metal and dielectric microparticles of submicron sizes from the surfaces of semiconductor devices. In view of the problem of surface laser cleaning, first calculations of laser radiation scattering from micrometer-sized dielectric particles were also performed [45–47]. The formation of a photonic nanojet was evidenced by those publications (see review [18]). The results of the corresponding studies became helpful later, when studying nanoablation [48–54]. Incidentally, the technology of forming nanoholes on a substrate covered by spherical microparticles was also developed as a result of studying the laser cleaning [46–48]. Figure 4 shows the view of a surface with an array of nanoholes formed on a substrate coated by a layer of micrometer-sized SiO_2 spheres, exposed to a laser pulse. Nanoholes up to 30 nm in diameter can be formed in this way [50].

The laser irradiation of a surface through an array of spherical particles also makes it possible to form arrays of nanobulges [51, 56] or nanohillocks with a height of 10–100 nm (Fig. 5), i.e., arrays of nanolenses [57]. Surfaces with nanobulges have many various applications, in particular, in magnetic recording [56].

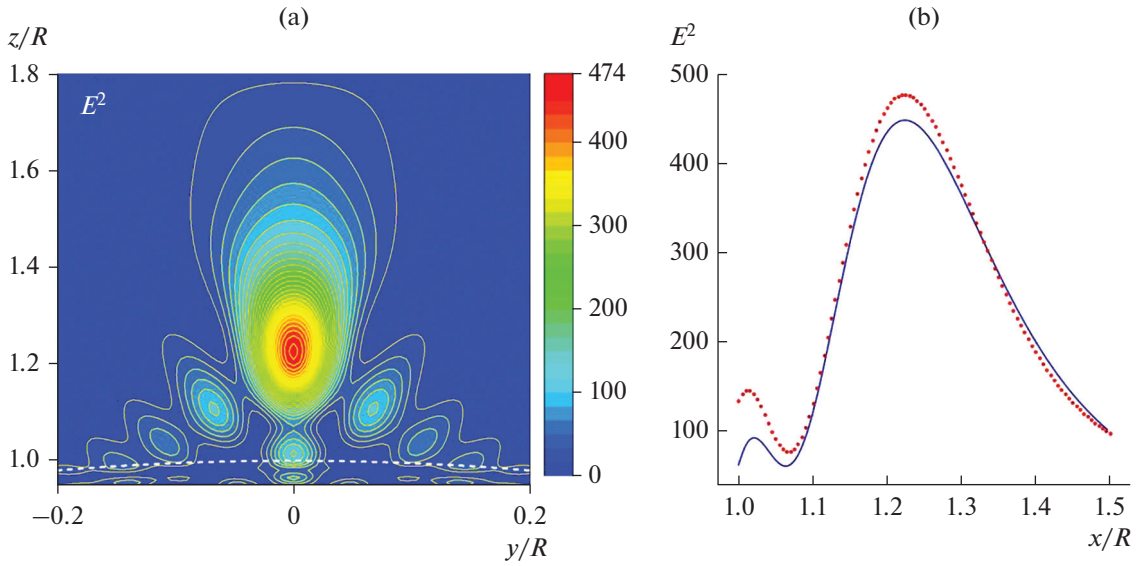

Fig. 3. (Color online) (a) Intensity distribution calculated according to the Mie theory with $n = 1.5$ and $q = 70$. This distribution is typical of the solution based on geometrical optics approximation (see, e.g., Fig. 5 in [11]). (б) Intensity distributions according to the Bessoid approximation [11] (solid blue line) and calculated according to the Mie theory (dotted red line).

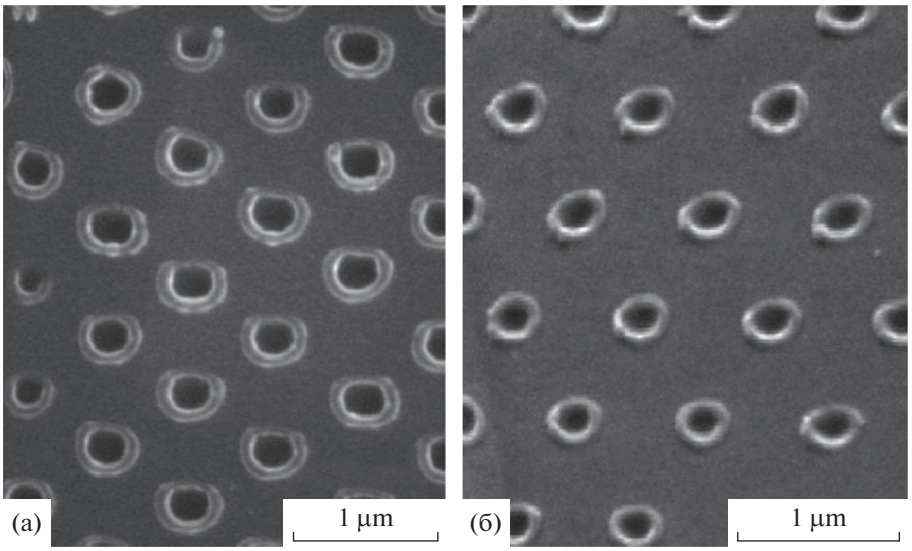

Fig. 4. Arrays of holes formed by a femtosecond pulsed laser beam (FWHM = 150 fs, λ = 800 nm) on a surface coated by a hexagonal colloidal monolayer of spherical particles: (a) silicon and (b) germanium substrates [49].

3. MAGNETIC LIGHT, NANOVORTICES, DIRECTED SCATTERING, AND FANO RESONANCES

About 400 years ago Rene Descartes suggested that the world space is saturated with giant solar whirlwinds, which make celestial bodies move. This concept was later criticized by Newton; nevertheless, it remained of interest for the public for a long time. For example, Ishmael, a character in Herman Melville's *Moby Dick*, ruminated about these whirlwinds while standing on board of the *Pequod*. From today's viewpoint, we can consider Descartes' ideas as precursors of singular optics, optical vortices, and optical tweezers. Indeed, it was discovered that light vortices can efficiently push particles; this discovery was awarded a Nobel prize.

In 1974 Nye and Berry introduced a new concept into the theory of waves: wavefront dislocations, objects arising as a result of the interference of light in the vicinity of singular points with zero Poynting vector [59–64]. These singular points in the phase plane are characterized by topological charges. The term

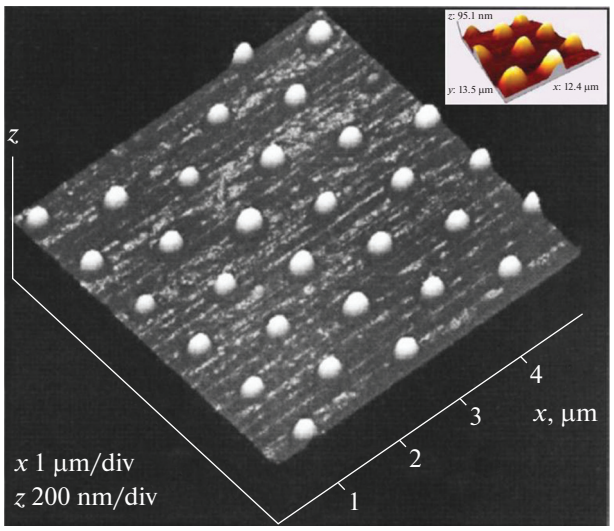

Fig. 5. (Color online) Silicon surface with nanobulges, formed as a result of silicon irradiation by a KrF laser pulse through an array of dielectric microspheres with a refractive index $n = 1.6$ [51].

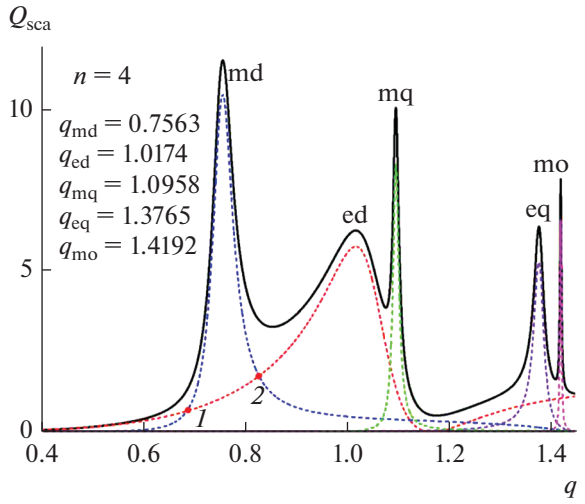

Fig. 6. (Color online) Dependence of the scattering efficiency Q_{sca} on the size parameter q for a sphere with a refractive index $n = 4$, calculated using the formulas of the Mie theory. The Mie resonances (dotted lines) are denoted as follows: (md) magnetic dipole, (ed) electric dipole, (mq) magnetic quadrupole, (eq) electric quadrupole, and (mo) magnetic octupole. The points at which the electric and magnetic dipoles become equal determine the scattering direction. Point 1 corresponds to the first Kerker condition, at which backscattering is suppressed completely. Point 2 corresponds to the second Kerker condition, with minimum forward scattering [75–77]. The scattering that is due to the electric dipole turns to zero at $q = 1.1654$.

optical vortices was introduced for these states in [59]. A number of methods for forming optical vortices are known in optics; they imply the use of Bessel, Laguerre–Gaussian, and other laser beams (see, e.g., [65]). The optical vortices formed by these methods have characteristic sizes on the order of light wavelength or larger [66]. Studies in the field of plasmonics revealed that light scattering from plasmonic nanostructures may lead to the formation of optical vortices with sizes much smaller than the light wavelength [67–73].

Optical vortices can be generated inside dielectric spheres [66]. It is convenient to observe these vortices in the Poynting vector distribution. Figure 6 shows the first five Mie resonances for scattering from a spherical particle with a refractive index $n = 4$ (Si at the boundary between the visible and IR spectral ranges [74]).

Figure 7 shows the values of electric (E^2) and magnetic (H^2) intensities, as well as the modulus of Poynting vector $|\mathbf{S}|$ and Poynting vector lines at the points of first five resonances in Fig. 6.

One can see characteristic scales of change in the corresponding fields at the Mie resonance points in the plots. A noteworthy feature is the fast increase in the magnetic intensity H^2 in comparison with the electric intensity E^2 at the magnetic resonance points: $H^2 = 663$, $E^2 = 25.4$ for the magnetic dipole, $H^2 = 1330$, $E^2 = 102$ for the magnetic quadrupole, and $H^2 = 3410$, $E^2 = 524$ for the magnetic octupole. One can easily see that the enhancement of magnetic intensity with respect to the electric intensity, H^2/E^2, is maximum for the magnetic dipole and decreases with an increase in the magnetic multipole order. Examples of vortices in the Poynting vector distribution for higher resonances are presented in Fig. 8.

The possibility of forming large magnetic moments during light scattering at optical frequencies in nanospheres with a high refractive index was predicted in theoretical studies [79, 80]. This phenomenon was soon confirmed experimentally [81, 82]. The presence of a large magnetic dipole moment allows one to implement directed scattering for particles with a small size parameter ($q << 1$). For these particles, the Rayleigh scattering caused by excitation of electric dipole moment is symmetric relative to the wave vector direction. Under these conditions, the maximum in the scattering diagram is directed aside with respect to the wave vector of the incident wave. Simultaneous excitation of electric and magnetic dipole moments makes it possible to form forward or backward scattering. The phenomenon of directed scattering for small (in comparison with the light wavelength) particles was experimentally confirmed in the microwave [83], visible [84], and IR [85] ranges. In essence, this was a confirmation of the possibility of designing high-efficiency nanoantennas [86].

The efficiencies of forward and backward light scattering (Q_{FS} and Q_{BS}, respectively) in the Mie theory are determined from the formulas

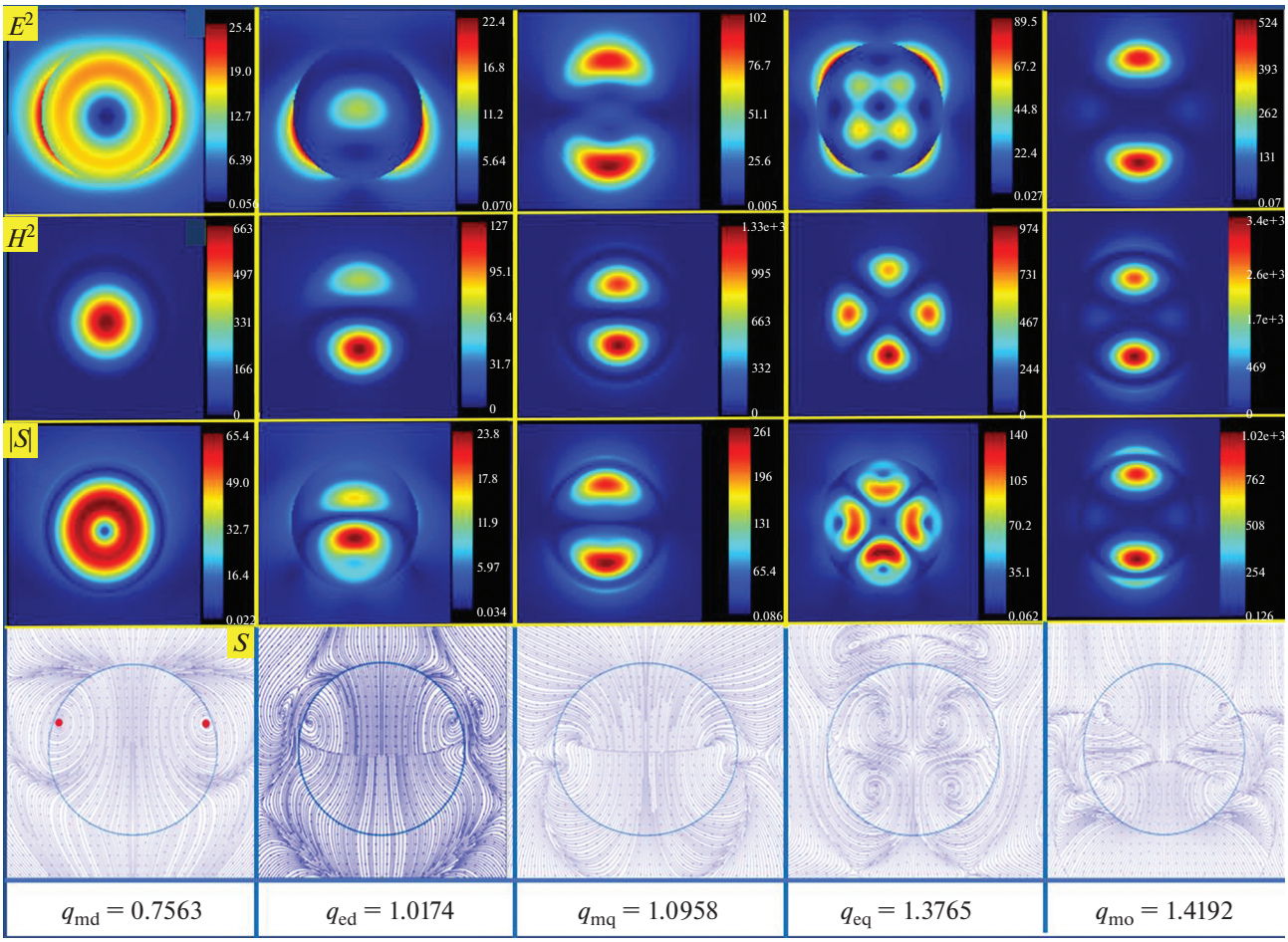

Fig. 7. Distributions of the electric intensity E^2 (first row), magnetic intensity H^2 (second row), Poynting vector modulus $|\mathbf{S}|$ (third row), Poynting vector lines (fourth row), and the resonant values of size parameter in the corresponding columns. The values for the first five resonances in Fig. 6 are indicated.

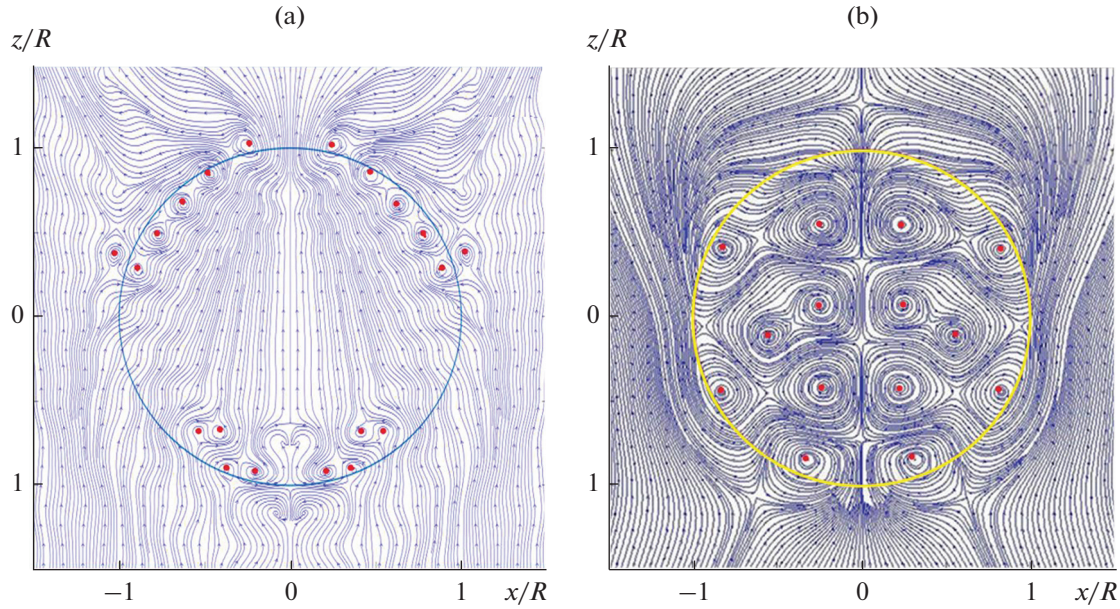

Fig. 8. (Color online) Poynting vector distributions for particles with refractive indices (a) $n = 1.5$, $q = 10$ [17] and (b) $n = 4$, $q = 2$ [78] in the range of high resonances with ℓ values on the order of 10.

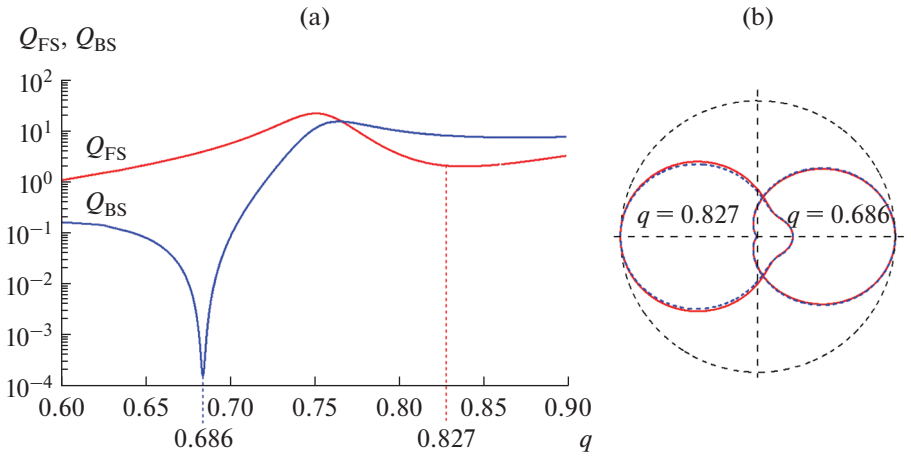

Fig. 9. (Color online) (a) Plots of the functions Q_{FS} (red line) and Q_{BS} (blue line) on a logarithmic scale for a particle with a refractive index $n = 4$. (b) The scattering diagrams in the minima of the corresponding functions. The left scattering diagram corresponds to the first Kerker condition (point 1 in Fig. 6), at which backscattering is suppressed completely. The right scattering diagram (point 2 in Fig. 6) corresponds to the second Kerker condition, with minimum forward scattering.

$$Q_{FS} = \frac{1}{q^2}\left|\sum_{\ell=1}^{\infty}(2\ell+1)(a_\ell + b_\ell)\right|^2,$$
$$Q_{BS} = \frac{1}{q^2}\left|\sum_{\ell=1}^{\infty}(2\ell+1)(-1)^\ell(a_\ell - b_\ell)\right|^2, \quad (8)$$

where the scattering amplitudes a_ℓ and b_ℓ are given by formulas (2).

The backward scattering for small particles is completely suppressed when $a_1 = b_1$. Since the scattering amplitudes are complex, this condition is a set of two equations. Figure 9 shows plots of the functions Q_{FS} and Q_{BS} and the scattering diagrams corresponding to the local minima of these functions.

Varying the size and shape of a particle, one can control both the amplitude and angular distribution of the scattering diagram [87–89]. Fano resonances play an important role in the light scattering by nanoparticles. These resonances, arising as a result of the interference of signals with wide and narrow spectra, are used in various physical, chemical, and biological applications [90–93]. The Q factor of Fano resonances increases for higher order modes; for example, the interference of the wide dipole (Rayleigh) mode and the narrow octupole mode in plasmonic particles provides a sharper resonance than the similar interference of dipole and quadrupole modes (see, e.g., Fig. 3 in [90]). Excitation of higher order Fano resonances [94–97] makes it possible to increase the sensitivity of resonant nanostructures. High-order (quadrupole, octupole, hexadecapole, and triacontadipole) Fano resonances, formed in an optimized plasmonic silver nanostructure with a disk ring, were demonstrated in [97]. However, the advance to resonances of even higher order in plasmonic nanostructures is limited by the dissipation effects in the visible range. In contrast, the dissipation effect may be weak in dielectric materials, due to which high-order Fano resonances can be implemented [78].

The main features of the Fano resonance can be understood by considering the classical problem of interaction of coupled oscillators [98, 99]. The existence of interference in this system is well known. This phenomenon is used, for example, in dynamic damping systems [100]. The dynamics of two coupled oscillators is described by their displacements from the equilibrium position, x_1 and x_2:

$$\ddot{x}_1 + \gamma_1\dot{x}_1 + \omega_1^2 x_1 = \Omega^2(x_2 - x_1) + f_1 e^{-i\omega t},$$
$$\ddot{x}_2 + \gamma_2\dot{x}_2 + \omega_2^2 x_2 = \Omega^2(x_1 - x_2) + f_2 e^{-i\omega t}. \quad (9)$$

Here, ω is the external force frequency, ω_1 and ω_2 are the eigenfrequencies, Ω is the oscillator coupling parameter, and γ_1 and γ_2 are the dissipation coefficients.

The steady-state solutions for the displacements are periodic functions: $x_1 = x_{10}\exp(-i\omega t)$ and $x_2 = x_{20}\exp(-i\omega t)$, where the amplitudes x_{10} and x_{20} are given by the expressions

$$x_{10} = \frac{(f_1 + f_2)\Omega^2 - f_1(i\gamma_2\omega + \omega^2 - \omega_2^2)}{(\omega_1^2 - \omega^2 - i\gamma_1\omega)(\omega_2^2 - \omega^2 - i\gamma_2\omega) - \Omega^4},$$
$$x_{20} = \frac{(f_1 + f_2)\Omega^2 - f_2(i\gamma_1\omega + \omega^2 - \omega_1^2)}{(\omega_1^2 - \omega^2 - i\gamma_1\omega)(\omega_2^2 - \omega^2 - i\gamma_2\omega) - \Omega^4}. \quad (10)$$

The paradigm of the classical analog of Fano resonance is as follows: light excites only a wide mode, for example, x_1, while a narrow resonance with a displacement x_2 (dark mode) is excited only due to the oscillator coupling [101, 102]. In this context, only one oscillator is driven by a harmonic force, so that we can assume that $f_2 = 0$. A specific example of this situation is shown in Fig. 10. The effects of both constructive (at

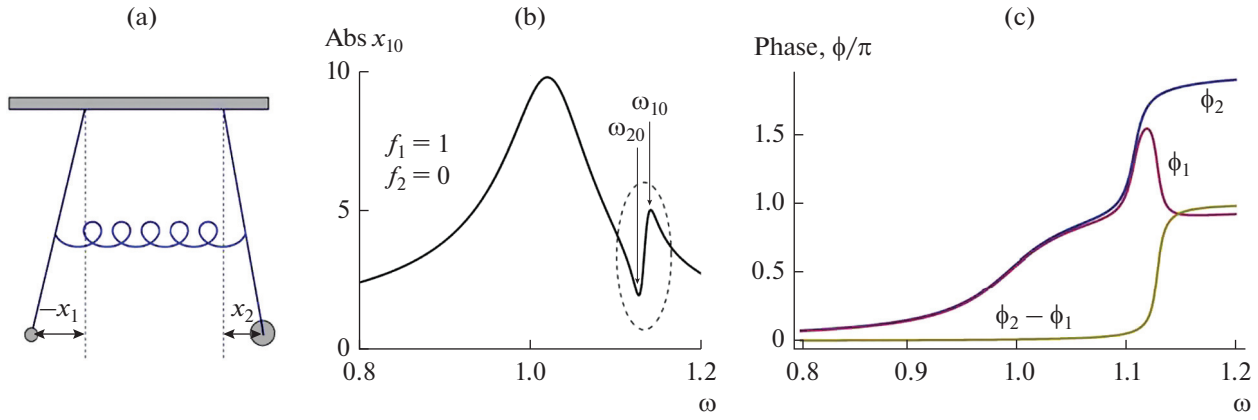

Fig. 10. (Color online) (a) Schematic diagram of two coupled oscillators. (b) The oscillator amplitude x_{10} was calculated from formulas (10) for $\omega_1 = 1$, $\omega_2 = 1.1$, $\Omega = 0.25$, $\gamma_1 = 0.1$, and $\gamma_2 = 0.01$. Correspondingly, constructive and destructive interference occurs at the resonant frequencies $\omega = \omega_{10}$ and $\omega = \omega_{20}$ (indicated by arrows). These frequencies lie in the vicinity of hybrid eigenfrequencies [98, 99]. (c) Phases of the first (ϕ_1) and second (ϕ_2) oscillators and their difference as a function of excitation frequency [103].

$\omega = \omega_{10}$) and destructive ($\omega = \omega_{20}$) interference can easily be identified in the resonance region. Note that a π phase jump arises for the second oscillator in the vicinity of Fano resonance (see Fig. 10c). Below the resonant frequency both displacements are in phase, while above the resonant frequency they oscillate in antiphase.

The coupled oscillator model was used to explain qualitatively many experimental results on Fano resonances (see, e.g., [103, 104]). However, to compare more adequately the theoretical and experimental data, one must solve numerically Maxwell's equations.

In the case of dielectric sphere, the high-order internal resonance mode interferes with the wide spectrum of all other modes. This effect is demonstrated in Fig. 11 for a particle with a refractive index $n = 1.5$ and a size parameter $q = 26.9419$. These parameters correspond to the resonant magnetic mode with $\ell = 35$. At the same time, the total number of modes taken into account for this size parameter in the Mie theory is $\ell_{\max} = 41$. Figure 11a shows the calculated field distribution in the $\{x, z\}$ plane, in which all modes with $\ell \le \ell_{\max}$ are taken into account. In Fig. 11b we present the same pattern, where all terms are taken into continuation, except for only the resonant term with $\ell = 35$. Thus, the only term with $\ell = 35$ leads to an increase in the scattered light intensity by a factor of 200.

The interference of wide and narrow spectral lines leads to a characteristic shape of Fano resonance for scattering in the far-field zone, as well as for the spectra of electric and magnetic field strengths on the particle surface at size parameters close to $q \approx 20$ (Fig. 12). Note that the characteristic shape of Fano resonances is observed also in the moduli on the scattering amplitudes [104]. The positions of the resonances in Figs. 12a and 12b coincide, but their amplitudes change by about 20% in the case of far-field scattering, whereas the amplitude of variations in the electric and magnetic field strengths is one to two orders of magnitude. The field intensities on the particle surface are presented in Fig. 12b, whereas inside the particle the fields may be an order of magnitude stronger. It follows from the analytical calculations [78] that the increase in the field strength within a particle for high-order Fano resonances may be as high as 10^9–10^{11}. The low energy dissipation in the material may also facilitate the field localization [105]. These high-order Fano resonances are promising for generating giant high-frequency magnetic fields inside dielectric particles [106]. Naturally, the size parameter must be larger for particles with a smaller refractive index than for the particles having a high refractive index. The typical range of the size parameters of interest is $q \approx 5$–50. For the visible spectrum, $q \approx 10$ corresponds to a particle size of about 10 μm. In microwave materials with a high permittivity ($\varepsilon > 100$) strong amplification of magnetic fields can be observed even in the range of the first Fano resonances [106].

Fano resonances and optical vortices are due to interference phenomena of different types. Generally these phenomena are independent. In many cases Fano resonances are observed without being bound to optical vortices, and the optical vortices are not accompanied by Fano resonances. However, when light is scattered from plasmonic nanoparticles, Fano resonances are accompanied by phase effects typical of singular optics [107]. In this case optical vortices with characteristic core sizes much smaller than the diffraction limit are formed. Surprisingly enough, it turned out that similar phenomena occur in dielectric particles with a size parameter $q \sim 10$.

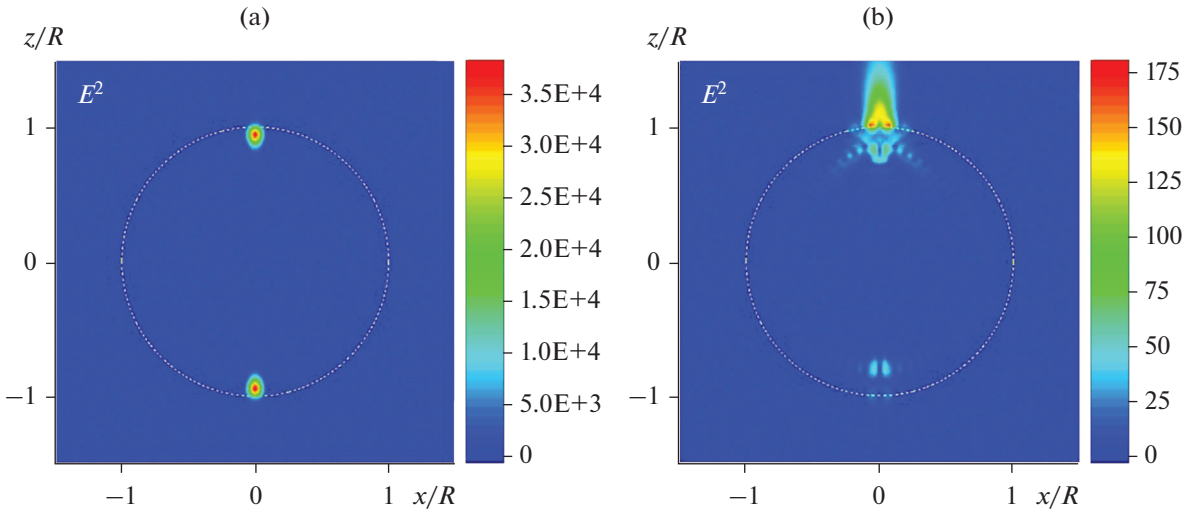

Fig. 11. (Color online) (a) Scattered-light intensity distribution in the $\{x, z\}$ plane, calculated according to the Mie theory with allowance for all terms with $\ell \le \ell_{max} = 41$, and (b) the same distribution disregarding the only resonant term with $\ell = 35$ [78].

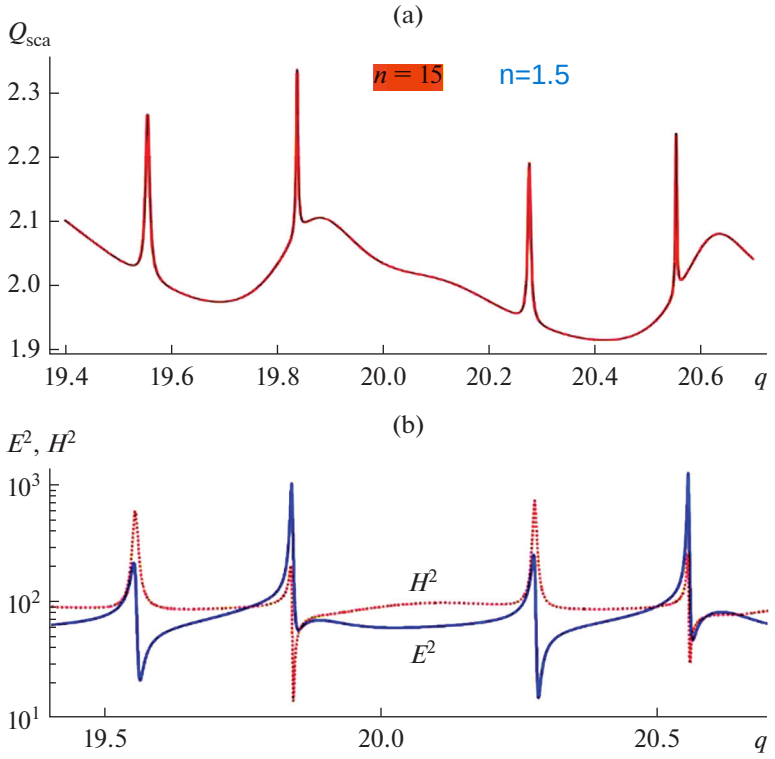

Fig. 12. (Color online) (a) Scattering efficiency for a particle with a refractive index $n = 1.5$ and size parameter close to $q \approx 20$ and (b) intensities of electric and magnetic fields on the surface of the same particle [78].

This phenomenon is explained within the theory of superoscillations [108–111], which is based on the following phenomenon: functions with a limited frequency range can oscillate more rapidly than their highest Fourier components [112, 113]. Due to this, fields can be localized on scales smaller than the diffraction scale according to the Abbe criterion: $\Delta x = \lambda/2n$. The local value of the wave vector of field inhomogeneity is related to the local phase gradient for this field, $k_{loc} = \nabla\Phi$ [113]. Singular optics is related to the formation of wavefront vortices and dislocations [58–66]. The key point of singular optics is the uncertainty

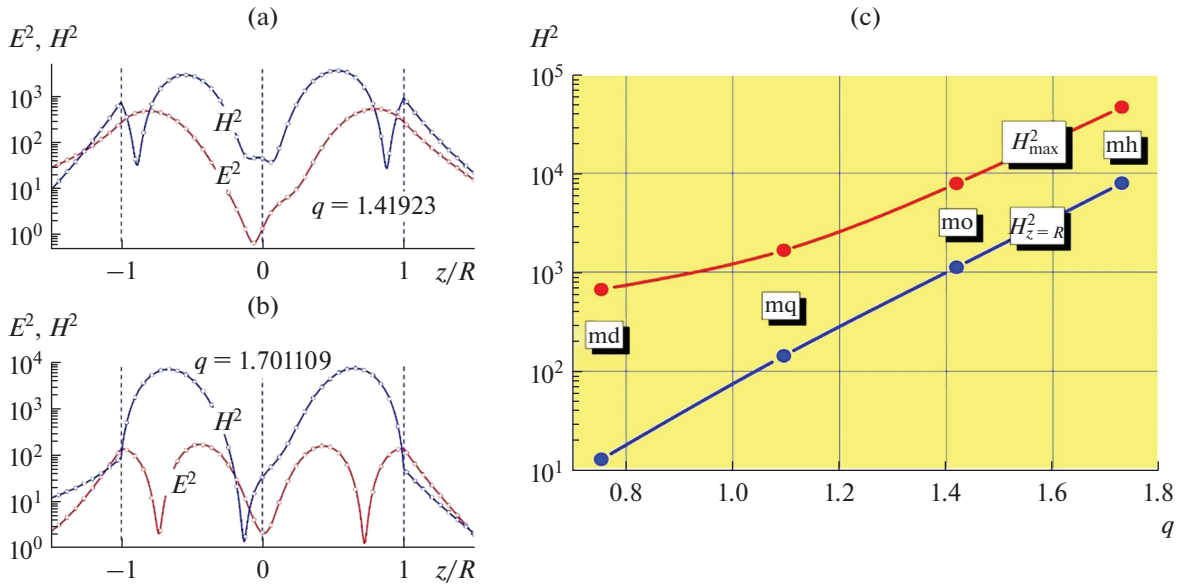

Fig. 13. (Color online) Electric and magnetic field distributions in a particle with a refractive index $n = 4$ and size parameters (a) $q = 1.41923$ (magnetic octupole resonance) and (b) $q = 1.70109$ (electric octupole resonance). One can see strong magnetic field enhancement in the particle. (c) Maximum values of magnetic intensity H^2 (normalized to the intensity in the incident wave) in a dielectric particle with a refractive index $n = 4$ (red dots) for the first four internal magnetic resonances. The plot shows the magnetic field strength on the particle surface at the wave emergence point (blue dots) [78].

of electromagnetic field phase at the points where the wave intensity is zero. At this point one can conjugate continuously any phase values differing by $2\pi m$, where the integer m is the so-called topological charge; it indicates the number of phase front twistings. There are many methods for forming optical vortices using diffraction, computer holograms, and spatial light modulators (see, e.g., [58–66]). These vortices can also be formed, for example, due to the light scattering by plasmonic nanostructures [67, 68]. In the case of weakly scattering plasmonic spheres, vortices can be observed even in the vicinity of dipole and quadrupole plasmon resonances (see examples in [67–73, 114]).

For small particles the Rayleigh approximation yields a scattering efficiency associated with the electric dipole resonance [6]:

$$Q_{\text{sca}} = \frac{8}{3}\left|\frac{\varepsilon - 1}{\varepsilon + 2}\right|^2 q^4. \tag{11}$$

Here, ε is the particle permittivity. This formula follows from the general formula of the Mie theory in the limit $q \ll 1$. Using this formula, Rayleigh explained the blue color of the sky [20]. However, Rayleigh's approximation (11) cannot be applied to weakly absorbing plasmonic particles. At the plasmon resonance frequency, when $\varepsilon \to -2$, the scattering cross section tends to infinity: $Q_{\text{sca}} \to \infty$. The Mie theory yields a correct (in the corresponding limit) value for partial scattering from the ℓth multipole resonance: $Q^{(\ell)}_{\text{sca}} = 2(2\ell + 1)/q^2$ [115, 116]. As a result, anomalous scattering with inverse hierarchy of optical resonances (the amplitude of quadrupole resonance exceeds that of the dipole resonance, the octupole resonance amplitude exceeds the quadrupole resonance amplitude, etc.) may occur in particles with low dissipation [117, 118].

A similar problem occurs in the case of Rayleigh approximation for the absorption of a small particle [6, 119]:

$$Q_{\text{abs}} = q\frac{12\varepsilon_2}{(\varepsilon_1 + 2)^2 + \varepsilon_2^2}, \tag{12}$$

where $\varepsilon = \varepsilon_1 + i\varepsilon_2$. One can easily see that formula (12) contains an uncertainty at $\varepsilon_2 \to 0$ at the plasmon resonance frequency $\varepsilon_1 \to -2$. In reality, anomalous absorption is implemented at certain low dissipations [120], at which a maximally possible (at $q \ll 1$) value is obtained:

$$Q^{(\ell)}_{\text{abs max}} = \frac{1}{q^2}\left(\ell + \frac{1}{2}\right). \tag{13}$$

This value is smaller by a factor of 4 than the maximum scattering intensity for the corresponding multipole: $Q^{(\ell)}_{\text{sca}} = 2(2\ell + 1)/q^2$. Anomalous absorption is obtained at different values of permittivity, depending on the particle size [120, 121]. For the dipole resonance, $\varepsilon_1 \approx -2 - 2.4q^2$, $\varepsilon_2 \approx 2q^3$. The anomalous absorption gives rise to the funnel effect [122], when a particle behaves as an attractor, collecting light from a large area and supplying it to the absorbing particle. This effect can be seen well in the Poynting vector dis-

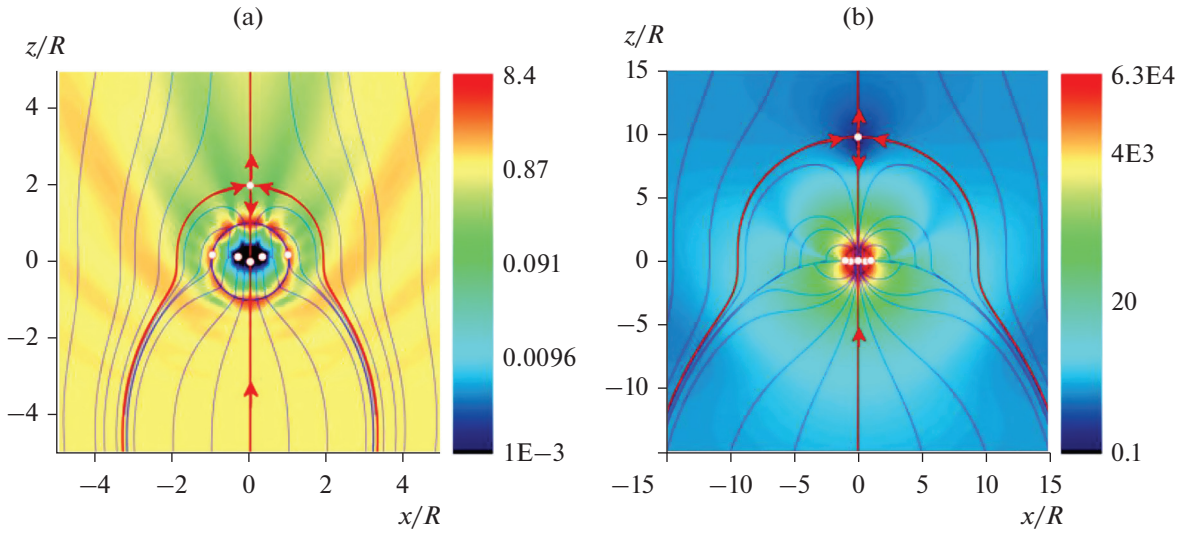

Fig. 14. (Color online) Poynting vector distribution in the xz plane for anomalous absorption in the vicinity of dipole resonance for plasmonic particles irradiated in vacuum. An incident linearly polarized plane wave propagates along the z axis with a vector $\mathbf{E}$ lying in the xz plane. The size parameter q is (a) 0.5 and (b) 0.1. The color density plots present Poynting vector modulus $|\mathbf{S}|^2$ (on the logarithmic scale). The Poynting vector lines are shown blue. The particle surface is denoted by a black line. Inside the particle div $\mathbf{S} < 0$; beyond the particle (in the free space) div $\mathbf{S} = 0$. The red lines in the plots denote separatrices, which illustrate the funnel effect. The white circles denote singularities: one saddle point is located above the particle, two singularities are located on the particle surface, and several stable nodes in the particle correspond to the absorption center positions [121].

tribution [65, 120, 121] (Fig. 14). As a result, the effective absorption area, πR_{eff}^2, becomes much larger than the geometric cross section πR^2. The smaller the particle size, the more pronounced this effect is. For the example presented in Fig. 14, $(R_{\text{eff}}/R)^2 \approx 10$ at $q = 0.5$ (Fig. 14a), while at $q = 0.1$ this value is about 300 (Fig. 14b).

The nanoparticle size and radiation wavelength at which anomalous absorption occurs can be determined for any real metal. The effective absorption coefficient α_{eff} of a particle under anomalous absorption conditions may significantly exceed its intrinsic absorption coefficient α. Thus, the effective absorption of weakly absorbing metals (K, Al, Na) can be increased by more than two orders of magnitude [121]. This is of interest for biomedical applications of nanoparticles [123].

4. ANAPOLE AND BOUND STATES IN CONTINUUM

In the last decade, the interest in various optical effects related to the so-called toroidal electrodynamics has been continuously increasing [124]. This interest is due to the specific features of the multipole response of the corresponding optical structures [125]. Here, one of the most interesting optical effects is the nonradiative state, the so-called anapole (toroidal dipole). This term, proposed by Ya.B. Zel'dovich [126], is related to a special distribution of charges and currents, which neither emits nor interacts with external fields. The toroidal dipole corresponds to currents flowing over the torus surface. It is convenient to study the effects of interaction of electric, magnetic, and toroidal dipoles in terms of multipole expansion in the Cartesian coordinate system [127]. All multipole modes are expressed in terms of integrals of different moments of current $\mathbf{j}$ over the particle volume. For example, the dipole moments can be written as [127]

$$p_{\text{i}} = \frac{i}{\omega}\int_V j_{\text{i}} d^3r, \quad m_{\text{i}} = \frac{1}{2}\int_V (\mathbf{r}\times\mathbf{j})_{\text{i}} d^3r,$$
$$T_{\text{i}} = \frac{1}{10}\int_V \left[(\mathbf{j}\times\mathbf{r})r_{\text{i}} - 2r^2 j_{\text{i}}\right] d^3r. \tag{14}$$

Here, p_{i} is the electric dipole, m_{i} is the magnetic dipole, and T_{i} is the toroidal dipole. The electric and toroidal dipoles turn out to have identical spatial distributions but different far-field phases (Fig. 15). The interference of these dipoles leads to vanishing scattering: the scattering object becomes invisible in the far field.

It can be seen in Fig. 6 that, at $n = 4$, the dipole scattering amplitude (red dotted line) turns to zero at the size parameter $q = 1.1654$. Note that the object remains visible in the near field. The anapole model was applied to describe dark matter in the Universe [128].

Since the times of Rayleigh, it is believed that even a very small particle can be seen because of light scattering; the minimum scattering is determined by formula (11). According to this formula, the ratio of the scattering efficiency to the fourth power of size param-

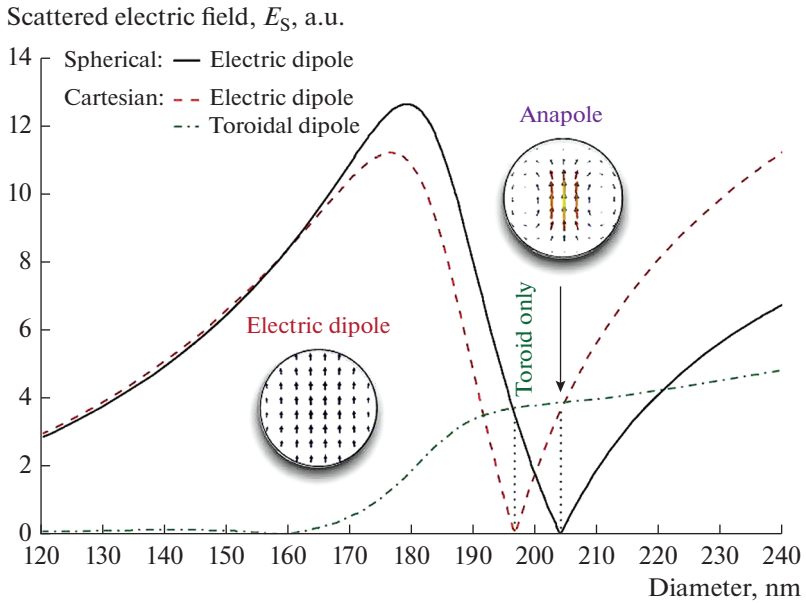

Fig. 15. (Color online) Spherical electric dipole according to the Mie theory at $n = 4$ and $\lambda = 550$ nm (black line), electric dipole in the Cartesian representation (red dotted line), and toroidal dipole moment (green dash-dotted line). For small spherical particles the contributions of spherical and Cartesian electric dipoles are identical, and the toroidal moment is small. For large particles one must take into account the contribution of the toroidal dipole moment. The anapole excitation is related to the disappearance of spherical electric dipole, when the Cartesian electric and toroidal dipoles compensate for each other [129].

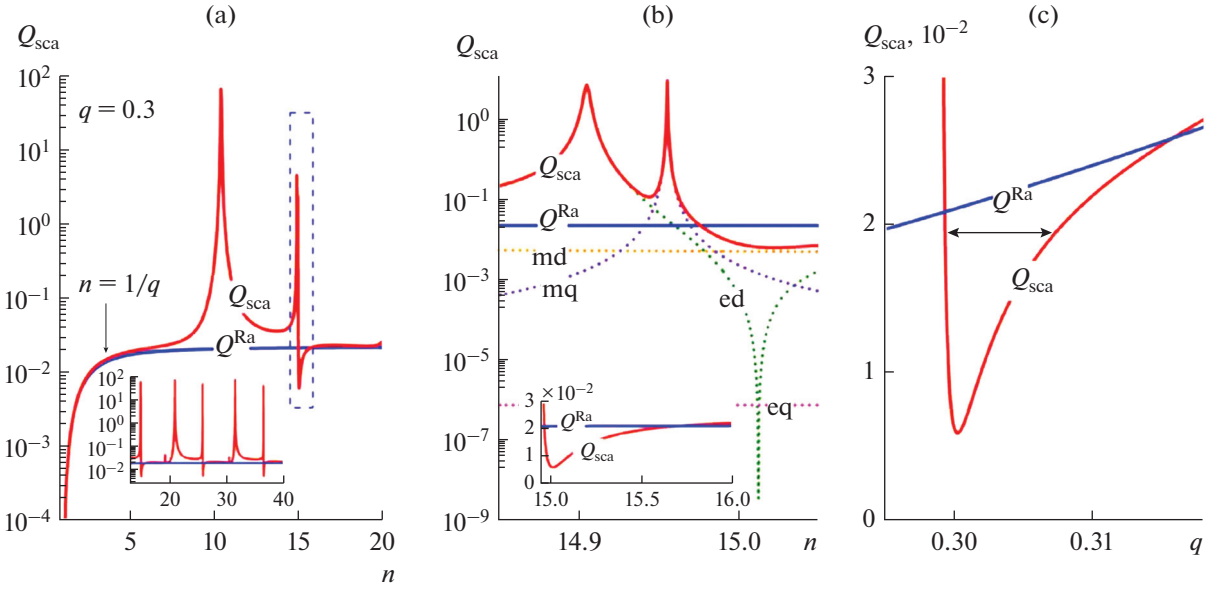

Fig. 16. (Color online) (a) Scattering efficiency of a spherical particle in correspondence with the Rayleigh approximation (blue line) and the exact result of the Mie theory (red line) for a small size parameter: $q = 0.3$. The inset in panel (a) shows resonances at higher refractive indices. In the vicinity of $n \approx 15, 26, 36$ the total scattering is less intense than it should be in accordance with Eq. (11). The region of suppressed scattering (dotted rectangle in panel (a)) is presented in more detail in panel (b), where the Rayleigh approximation (blue line) and exact value given by the Mie theory (red line) are shown jointly with four particular scattering coefficients for the magnetic dipole (md), electric dipole (ed), magnetic quadrupole (mq), and electric quadrupole (eq).

The inset in panel (b) shows the range $Q_{sca} < Q_{sca}^{(Ra)}$, extended from $n = 15.0$ to $n = 15.7$. (c) The range $Q_{sca} < Q_{sca}^{(Ra)}$ as a function of size parameter at $n = 15.0$ [130].

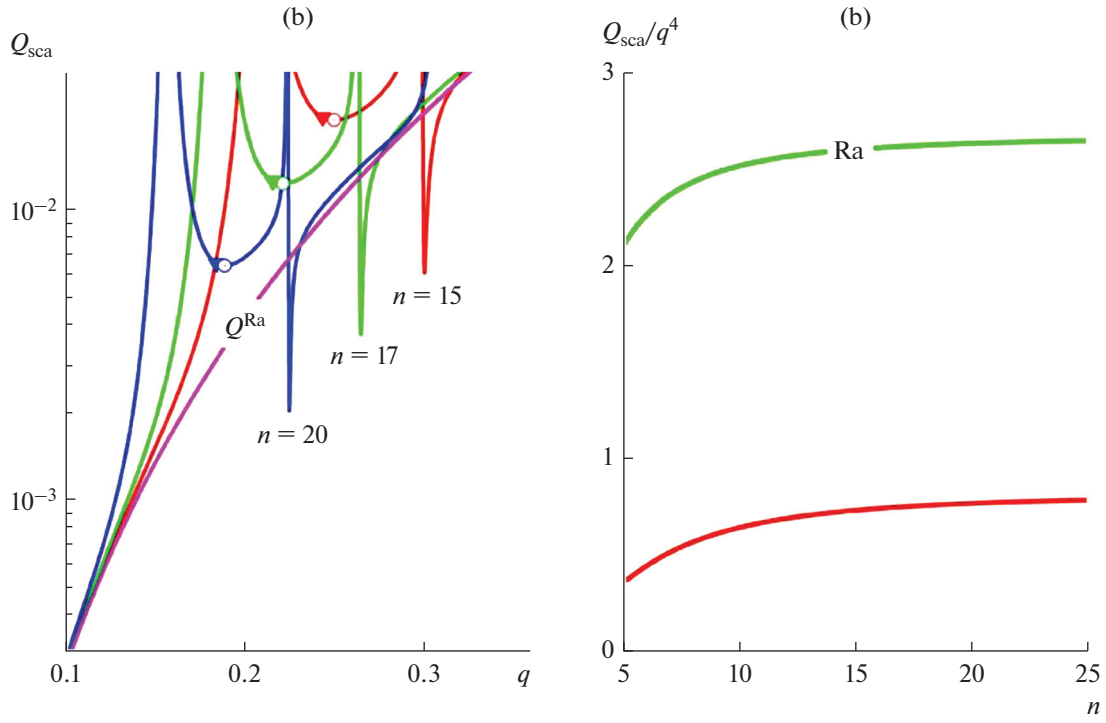

Fig. 17. (Color online) (a) Dependence of the scattering efficiency on the size parameter for three refractive indices: $n = 15$ (red), 17 (green), and 20 (blue). Open circles show the positions of local scattering minima. Triangles indicate the spread at the points corresponding to minimum forward scattering under the second Kerker condition. (b) Dependence of $Q_{sca}^{(Ra)}/q^4$ on the refractive index along the directions of Rayleigh scattering (green line) and anapole mode (red line) [130].

eter is a universal function, which increases monotonically with an increase in refractive index at $n > 1$:

$$\frac{Q_{sca}^{(Ra)}}{q^4} = \frac{8}{3}\left|\frac{\varepsilon - 1}{\varepsilon + 2}\right|^2. \qquad (15)$$

In the case of Rayleigh scattering the main contribution to scattering is from the electric dipole mode. The contribution from all other multipoles is much smaller. However, the interference between the electric and toroidal dipoles may suppress Rayleigh scattering [130]. This suppression occurs when $Q_1^{(e)} = 0$ (which is equivalent to $\Re_1^{(a)} = 0$). This condition is satisfied along the trajectory determined by the equation [131]

$$\begin{aligned} &1 - n^2 + q(n^2 - 1 + n^2q^2)\cot(q) \\ &+ nq(n^2 - 1 - n^2q^2)\cot(nq) \\ &+ nq^2(1 - n^2)\cot(q)\cot(nq) = 0. \end{aligned} \qquad (16)$$

Here, we consider only those solutions to Eq. (16) for which $\cos(q) \neq 0$ and $\cos(nq) \neq 0$.

It is no surprise that the particle scattering efficiency near resonances is much higher than in the case of Rayleigh scattering. However, the asymmetric shape of resonance line (Fig. 16a) also leads to strong suppression of total scattering near the resonance, which becomes smaller than that given by Rayleigh formula (11). This effect is observed, for example, in the vicinity of $n \approx 15$ (area outlined by a dotted line in Fig. 16a). This area on a larger scale is shown in Fig. 16b. It can be seen in the plot that there are two closely spaced resonances: electric dipole and magnetic quadrupole, which are not resolved on the scale of Fig. 16a. Despite the fact that there are many points with local scattering minima, as demonstrates the inset in Fig. 16a, a more accurate consideration within the Mie theory shows that the global minimum of scattering is obtained in the resonance minimum near $n \approx 15$. The total scattering efficiency $Q_{sca} \approx 5.99 \times 10^{-3}$ for a particle with this refractive index is lower by a factor of about 3.5 than for the Rayleigh scattering calculated from formula (11), $Q_{sca}^{(Ra)} \approx 2.11 \times 10^{-2}$. A detailed analysis of this resonance [130] shows that its shape is typical of a Fano resonance with a narrow transmission band, as presented in Fig. 16a.

When exciting an anapole mode, scattering less intense than the corresponding Rayleigh scattering can be implemented (Fig. 17). It is noteworthy that the anapole mode yields the global scattering minimum. The minimization of only differential scattering does not minimize total scattering. For example, the minimization of forward scattering (provided that the sec-

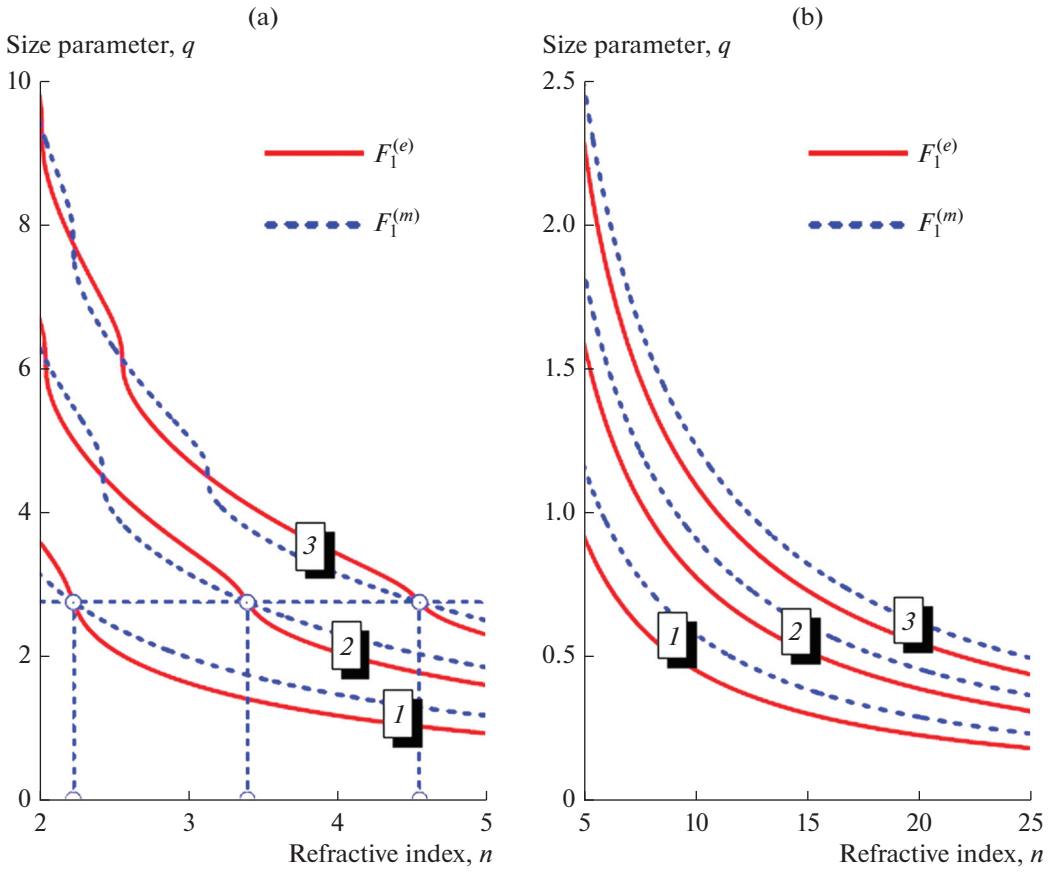

Fig. 18. (Color online) Trajectories $F_1^{(e)}(n,q) = 0$ (equivalent of $\Re_1^{(a)} = 0$) and $F_1^{(m)}(n,q) = 0$ (equivalent of $\Re_1^{(b)} = 0$), corresponding to the disappearance of electric and magnetic dipole modes in the plane of parameters n and q, for (a) $n < 5$ and (b) $n > 5$.

ond Kerker condition is satisfied) approaches to a local minimum in scattering (Fig. 17a), but the intensity of this scattering is nevertheless higher than that of Rayleigh scattering. The global scattering minimization is explicitly visualized in Fig. 17c, where the parameter $Q_{\text{sca}}^{(Ra)}/q^4$ as a function of particle refractive index is shown for the Rayleigh approximation and for the global minimum related to the anapole mode excitation.

The anapole mode was observed experimentally in the microwave range for a metamaterial whose unit cell contained four split wire loops, inserted in a dielectric plate [132], as well as in the optical range for silicon nanocylinders [129], in plasmonic devices [133], and in many other systems [79, 134–154].

A hybrid situation was discussed in [131], where electric and magnetic anapole modes were excited simultaneously at the same frequency. Similar to Eq. (16), one can determine the trajectory of the curve along which $Q_1^{(m)} = 0$:

$$n^2 - 1 + nq\left[\cot(nq) - n\cot(n)\right] = 0, \qquad (17)$$

which is equivalent to $\Re_1^{(b)} = 0$.

The plots of the curves (16) and (17) are presented in Fig. 18. One can see that, at certain n and q values, one can simultaneously turn to zero the contributions of both electric and magnetic dipole scatterings.

The field distributions in the case of electric and magnetic anapoles differ qualitatively (Fig. 19). Figure 19a (top) shows the electric vector distribution inside a nanoparticle. The white lines are electric field force lines. A poloidal current can be seen well in this distribution. The Poynting vector distribution in the $\{x, z\}$ plane is shown in Fig. 19b. Note that the energy flux is almost absent in the region of separatrice loops around the focal points 3 and 4. The electric anapole is equivalent to the confocal system of two lenses with a numerical aperture (NA) close to unity.

The lower plot in Fig. 19a presents the distribution of magnetic field intensity H^2 in the $\{y, z\}$ plane. White lines are the force lines of the magnetic field vector **H**. The plot demonstrates a poloidal distribution of magnetic field in the nanoparticle. Figure 19b (bottom) shows that, in contrast to the electric anapole, where energy is "captured" into the particle, the energy in the magnetic anapole is "pushed out" beyond the par-

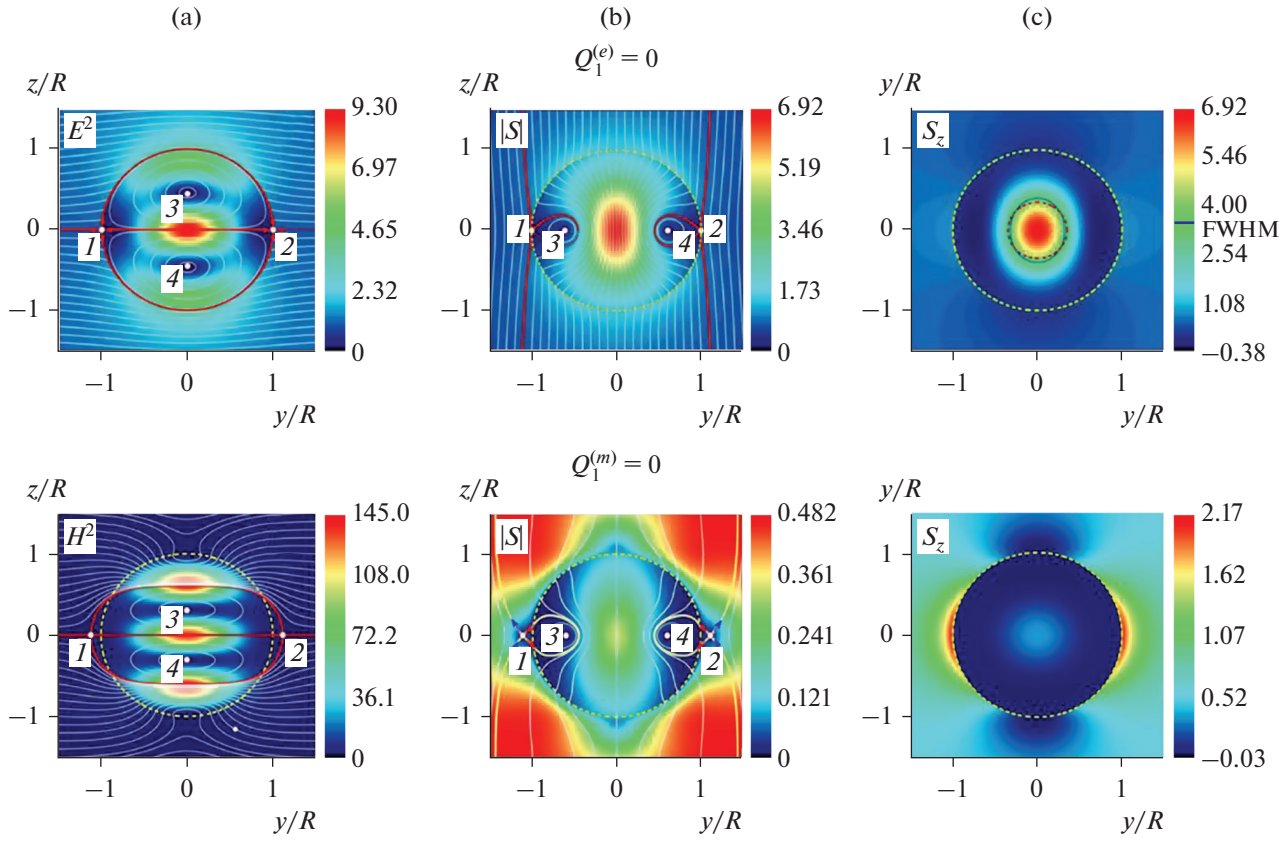

Fig. 19. (Color online) The patterns in the upper row correspond to an electric anapole with $Q_1^{(e)} = 0$ ($q = 0.17988$ and $n = 25$): distributions of the (a) electric field $\mathbf{E}^2$, (b) Poynting vector modulus in the $\{x, z\}$ plane, and (c) z component of the Poynting vector in the $\{x, y\}$ plane along the particle diameter. The red dotted line shows the diffraction limit $\pi/2qn \approx 0.35$, and the blue line indicates the FWHM value for intensity. Similar distributions in the lower row correspond to a magnetic anapole with $Q_1^{(m)} = 0$: $q = 0.23062$ and $n = 25$ [131].

ticle and a near field (similar to a plasmonic particle) is formed. This can be seen well in Fig. 19c (bottom).

Thus, simultaneous destructive interference of the electric, magnetic, and corresponding toroidal dipole modes (the so-called hybrid anapole mode) can be achieved for a spherical particle by changing the refractive index and/or size of this particle. However, the number of degrees of freedom in spherical geometry is insufficient to expand the effect of hybrid anapole mode to higher multipoles. In view of the optical theorem, it is also impossible to develop an ideal anapole with destructive interference for all multipoles when a particle is exposed to plane waves. In principle, radiative loss can be suppressed for a finite number of multipoles, using a nanoantenna of complex geometry. A possibility of exciting the hybrid anapole state in a dielectric particle, providing suppression of both the dipole and quadrupole electric and magnetic scatterings, was demonstrated in [153]. This hybrid state can be excited in a particle shaped as a triaxial ellipsoid with semiaxes $\{a, b, c\}$ by choosing appropriate side ratios b/a and c/a, as well as the refractive index n and size parameter $q = 2\pi a/\lambda$. An example of this state is shown in Fig. 20.

Anapole states correspond to the suppression of far-field scattering; they provide simultaneously energy concentration in subwavelength volumes, which was confirmed experimentally [154]. This effect is used to enhance nonlinear interactions in nanostructures (see numerous examples in [139, 154–163]).

Figure 21 shows a possible anapole laser design proposed in [159]. Recently this concept was implemented experimentally for active dielectric metasurfaces, consisting of InGaAsP nanodisks with built-in quantum wells [164]. Low-threshold room-temperature lasing was demonstrated for a metasurface composed of anapole lattices.

Another type of interference phenomena arises when there is a strong coupling between the radiative modes maintained by subwavelength dielectric cavity with a high refractive index. In this case, resonances due to the continuum bound states arise [141, 165]. The nature of these resonances is related to the disappearance of the relationship between the resonant

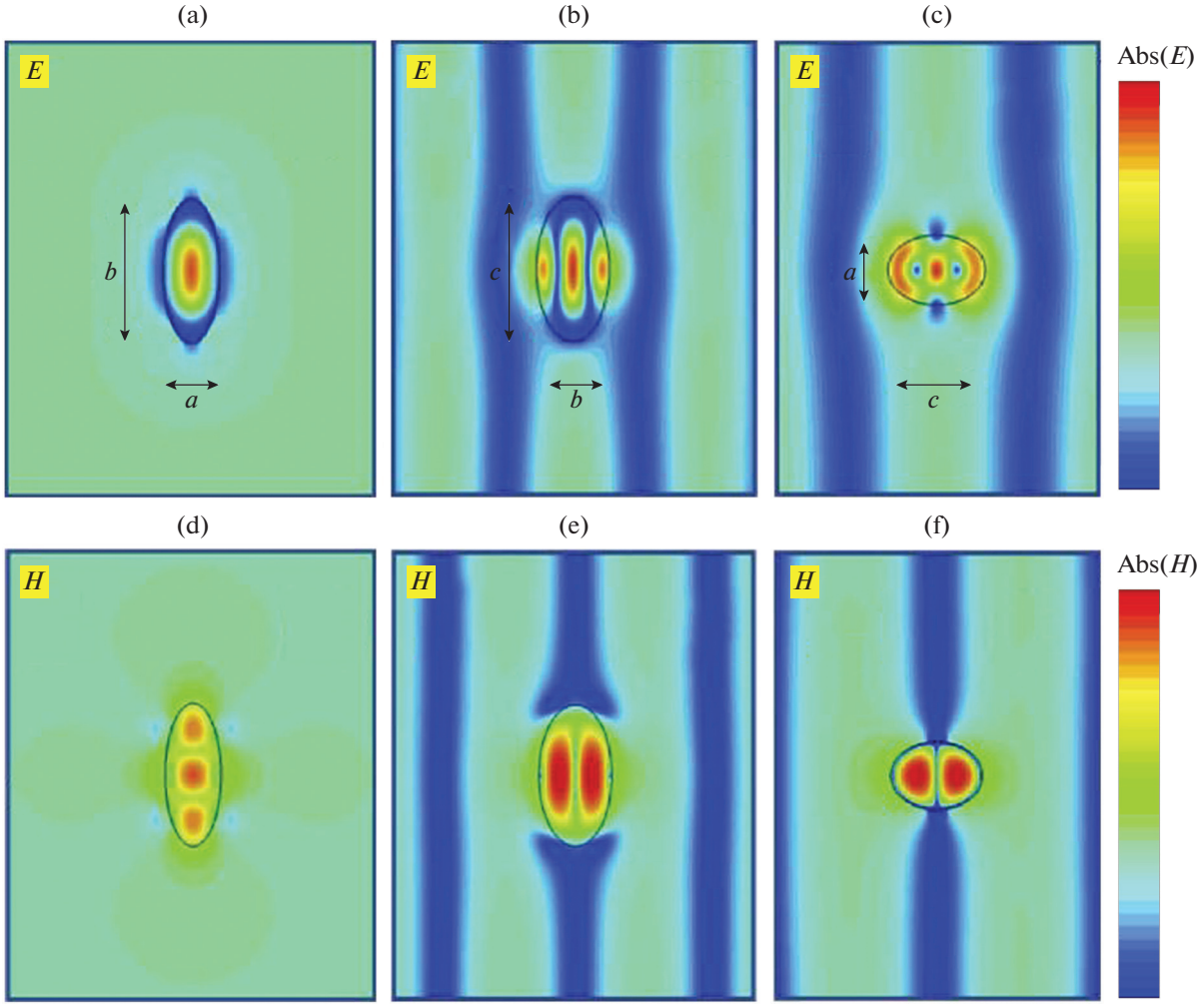

Fig. 20. (Color online) Distributions of electric and magnetic fields in the (*a*, *d*) *xy*, (*b*, *e*) *yz*, and (*c*, *f*) *xz* planes for an ellipsoidal particle with the axes $a = 0.7R$, $b = 1.85R$, and $c = R$ at a refractive index $n = \sqrt{30}$ and size parameter $q = 0.85$. The position of magnetic quadrupole resonance can be shifted using additionally a thin substrate with a low permittivity: $\varepsilon = 1.5$ [153].

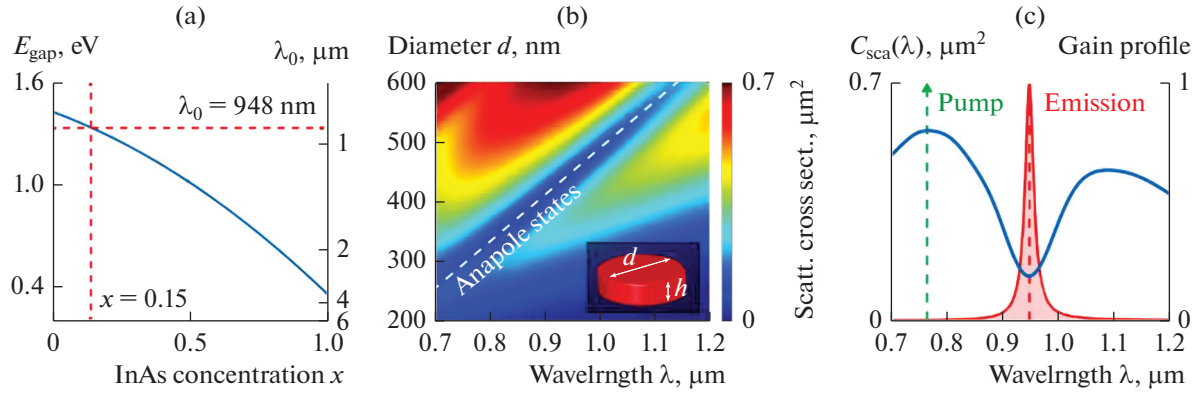

Fig. 21. (Color online) (a) Dependence of the $In_xGa_{(1-x)}As$ band gap on the molar ratio *x* InAs. (b) Scattering cross section of an $In_{0.15}Ga_{0.85}As$ nanodisk in dependence of the disk diameter *d* and incident wavelength λ. The white dotted line indicates the region in which scattering is suppressed due to the presence of anapole states. (c) Scattering cross section of an $In_{0.15}Ga_{0.85}As$ nanodisk with a diameter $d = 440$ nm and a height $h = 100$ nm. The red hatched area shows the profile of emission enhancement in the scattering suppression range [159].

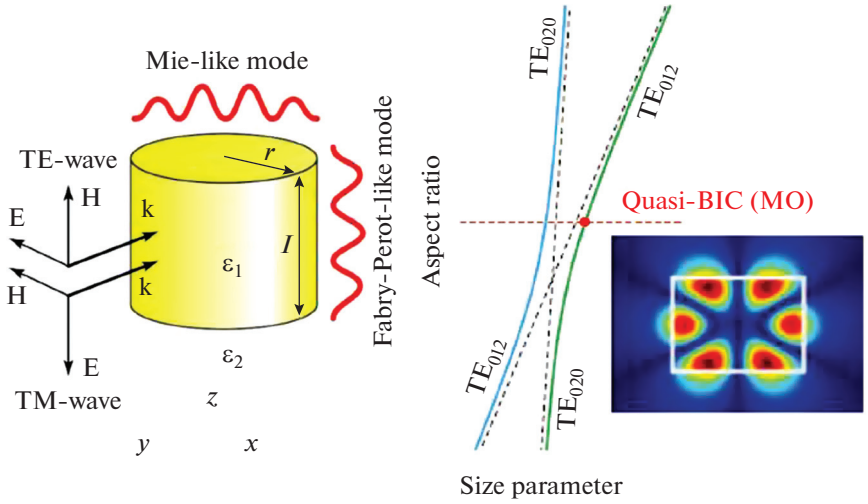

Fig. 22. (Color online) Strong mode coupling in a subwave dielectric cavity with occurrence of quasi-localized state. Frequencies of the Mie mode TE_{020} and Fabry–Perot mode TE_{012} in the avoided-crossing regime for the modes with an azimuthal number $m = 0$ [165].

mode and all environmental radiative channels. The possibility of this resonance was discussed theoretically almost 100 years by von Neumann and Wigner [166]. There are approximately ten different mechanisms of the occurrence of these localized states in the continuum. Of special interest for photonics turned out to be the Friedrich–Wintgen mechanism [167], where two modes of the same symmetry for the same structure come closer with a change in the parameters of the system. At the instant of anticrossing these modes are in antiphase and compensate for each other, emitting in the same radiative channel. A great number of studies have been devoted to these structures (see reviews [139, 168–171]). For example, there are two modes in a subwavelength dielectric cavity: one is related to the Mie resonances in an infinite cylinder and the other is related to the Fabry–Perot resonances upon reflection from the cylinder end faces [165] (Fig. 22). The intersection of these modes with a change in the cylinder height/diameter ratio and the size parameter provides conditions for the formation of quasi-localized state with magnetic octupole symmetry in the continuum.

The formation of quasi-localized modes in the continuum is promising for many applications. For example, a possibility of designing a laser operating at the frequency of quasi-localized modes was demonstrated in [170]. In our previous study [171] it was shown that a bound state in the continuum makes it possible to significantly enhance the magneto-optical response of the system.

5. CONCLUSIONS

The following three ranges of size parameters $q = 2\pi R/\lambda$ (R is the characteristic size of scattering object, λ is the incident radiation wavelength) are generally distinguished in modern optics: (1) $q \ll 1$, which corresponds to the Rayleigh scattering of small particles; (2) $q \sim 1$, range of Mie resonances (generally, dipole, quadrupole, and octupole resonances, which form a section of modern plasmonics and nanophotonics [12]) or mesoscopic range; and (3) $q \gg 1$, the range of geometric optics. The latter range for typical optical materials (glass, quartz, etc.) covers very large sizes: $q \geq 100$ [11].

When scattering occurs from an isolated dielectric nanoantenna [86] and dielectric nanostructures, in contrast to plasmonics, both electric and magnetic multipole modes can be excited. In this case, along with the conventional Fano resonances, there is a variety of new resonant effects caused by interference. These phenomena, often referred to as Kerker effects, lie in the basis of some new resonant properties of dielectric nanoantennas and metasurfaces. Control of resonant multipole excitation of dielectric particles and interference of electric and magnetic multipoles is a key element in designing resonant dielectric metadevices. Dielectric particles of even simple shape allow for excitation of a rich variety of electric and magnetic multipole resonances in them. Phases and amplitudes of these resonances can be controlled by changing the size and shape of particles, as well as the environmental parameters. This control makes it possible to enhance or suppress light scattering in certain directions and form complex scattering diagrams using multipole interference.

The range of intermediate values of size parameter, $q \sim 10$, had remained a terra incognita in the field of optics for a long time; however, a number of new optical effects have been discovered in this field in the last years: optical and magnetic nanojets [17], optical

nanovortices of subwavelength sizes [73], anapole nonradiative optical structures [131], high-order Fano resonances with generation of superstrong magnetic fields [78, 106], etc. In this context the values $q \sim 10$ can be selected as a characteristic range of peculiar optical phenomena, caused by the effects of magnetic field localization. Even a new term was proposed for this range: "optics of dielectric mesoscale particles" [172] or "mesoscopic optics."

FUNDING

B.L., A.B., and A.F. acknowledge the support of the Program for Development of Moscow State University, the Russian Science Foundation (project no. 20-12-00389), and the Russian Foundation for Basic Research (project no. 20-02-00715). Z.W. acknowledges the support from the European Regional Development Fund (ERDF) and the Welsh European Funding Office (WEFO) (SPARCII c81133). I.M. and O.M. acknowledge the support of the Program for Development of the Tomsk Polytechnical University.

CONFLICT OF INTEREST

The authors declare that they have no conflicts of interest.

REFERENCES

1. G. Mie, "Beiträge zur Optik trüber Medien, speziell kolloidaler Metallösungen," *Ann. Phys.* **25**, 376–445 (1908). https://doi.org/10.1002/andp.19083300302
2. N. A. Logan, "Survey of some early studies of the scattering of plane waves by a sphere," *Proc. IEEE* **53** (8), 773–785 (1965). https://doi.org/10.1109/PROC.1965.4055
3. S. Mayer, *Plasmonics: Fundamentals and Applications* (Springer, New York, 2007). https://doi.org/10.1007/0-387-37825-1
4. V. Klimov, *Nanoplasmonics* (*Pan Stanford, New York*, 2014). **ISBN-10**: 9814267163.
5. Z. Wang, B. Luk'yanchuk, L. Yue, R. Paniagua-Domínguez, B. Yan, J. Monks, O. V. Minin, I. V. Minin, S. Huang, and A. A. Fedyanin, "Super-resonances in microspheres: Extreme effects in field localization," *arXiv:1906.09636* (2019).
6. C. F. Bohren and D. R. Huffmann, *Absorption and Scattering of Light by Small Particles* (Wiley–Interscience, New York, 2004). https://doi.org/10.1002/9783527618156
7. P. W. Barber and S. C. Hill, *Light Scattering by Particles: Computational Methods* (World Sci., Singapore, 1990). https://doi.org/10.1142/0784
8. Y. A. Kravtsov and Y. I. Orlov, *Geometrical Optics of Inhomogeneous Media* (Springer, Berlin, 1990). ISBN-10: 3642840337.
9. T. Pearcey, "The structure of an electromagnetic field in the neighborhood of a cusp of a caustic," *Philos. Mag.* **37**, 311–317 (1946). https://doi.org/10.1080/14786444608561335
10. M. V. Berry and C. J. Howls, "Integrals with coalescing saddles," in *NIST Handbook of Mathematical Functions* (Cambridge Univ. Press, Cambridge, 2010), Chap. 36, pp. 775–793. ISBN 978-0-521-19225-5.
11. J. Kofler and N. Arnold, "Axially symmetric focusing as a cuspoid diffraction catastrophe: Scalar and vector cases and comparison with the theory of Mie," *Phys. Rev. B* **73**, 235401 (2006). https://doi.org/10.1103/PhysRevB.73.235401
12. A. I. Kuznetsov, A. E. Miroshnichenko, M. L. Brongersma, Y. S. Kivshar, and B. Luk'yanchuk, "Optically resonant dielectric nanostructures," *Science* **354** (6314), aag2472 (2016). https://doi.org/10.1126/science.aag2472
13. R. Paniagua-Domingues, B. Luk'yanchuk, and A. I. Kuznetsov, "Control of scattering by isolated dielectric nanoantennas," in *Dielectric Metamaterials: Fundamentals, Designs, and Applications* (Elsevier, Netherlands, 2020), Chap. 3, pp. 73–108. https://doi.org/10.1016/B978-0-08-102403-4.00008-6
14. D. V. Obydennov, D. A. Shilkin, E. I. Elyas, V. V. Yaroshenko, O. S. Kudryavtsev, D. A. Zuev, E. V. Lyubin, E. A. Ekimov, I. I. Vlasov, and A. A. Fedyanin, "Spontaneous light emission assisted by Mie resonances in diamond nanoparticles," *Nano Lett.* **21**, 10127 (2021). https://doi.org/10.1021/acs.nanolett.1c02616
15. A. Kwan, J. Dudley, and E. Lantz, "Who really discovered Snell's law?" *Phys. World* **15** (4), 64 (2002). https://doi.org/10.1088/2058-7058/15/4/44
16. V. I. Arnold, "On teaching mathematics," *Russ. Math. Surveys* **53** (1), 229–236 (1998).
17. B. S. Luk'yanchuk, R. Paniagua-Domınguez, I. V. Minin, O. V. Minin, and Z. B. Wang, "Refractive index less than two: Photonic nanojets yesterday, today and tomorrow," *Opt. Mater. Express* **7** (6), 1820–1847 (2017). https://doi.org/10.1364/OME.7.001820
18. V. I. Arnold, *Catastrophe Theory* (Springer Science & Business Media, 2003). https://doi.org/10.1007/978-3-642-96799-3
19. T. Poston and I. Stewart, *Catastrophe Theory and Its Applications* (Courier Corp., 2014).
20. B. Luk'yanchuk, N. Arnold, S. M. Huang, Z. B. Wang, and M. H. Hong, "Three-dimensional effects in dry laser cleaning," *Appl. Phys. A* **77**, 209–215 (2003). https://doi.org/10.1007/s00339-003-2139-z
21. J. W. Strutt (Lord Rayleigh), "On the light from the sky, its polarization and colour," *Philos. Mag.* **41**, 447–454 (1871). https://doi.org/10.1080/14786447108640452
22. I. V. Minin, O. V. Minin, Y. Cao, B. Yan, Z. Wang, and B. Luk'yanchuk, "Photonic lenses with whispering gallery waves at Janus particles," *Opto-Electron. Sci.* **1** (2), 210008 (2022). https://doi.org/10.29026/oes.2022.210008
23. I. V. Minin, Y. E. Geints, A. A. Zemlyanov, and O. V. Minin, "Specular-reflection photonic nanojet: Physical basis and optical trapping application," *Opt. Express* **28**, 22690 (2020). https://doi.org/10.1364/OE.400460
24. Z. Chen, A. Taflove, and V. Backman, "Photonic nanojet enhancement of backscattering of light by nanoparticles: A potential novel visible-light ultrami-

croscopy technique," *Opt. Express* **12**, 1214–1220 (2004).
https://doi.org/10.1364/OPEX.12.001214

25. A. J. Littlefield, J. Zhu, J. F. Messinger, and L. L. Goddard, "Photonic nanojets," *Opt. Photonics News* **32** (1), 34–41 (2021).
https://doi.org/10.1364/OPN.32.1.000034
26. P. Zhang, B. Yan, G. Gu, Z. Yu, X. Chen, Z. B. Wang, and H. Yang, "Confining photonic nanojet in a microwell on microsphere lens for highly efficient light focusing, signal amplification and quantitative detection," *arXiv:2107.04115* (2021).
https://doi.org/10.48550/arXiv.2107.04115
27. W. Wu, A. Katsnelson, O. G. Memis, and H. Mohseni, "A deep sub-wavelength process for the formation of highly uniform arrays of nanoholes and nanopillars," *Nanotechnology* **18**, 485302 (2007).
https://doi.org/10.1088/0957-4484/18/48/485302
28. E. McLeod and V. Arnold, "Subwavelength direct-write nanopatterning using optically trapped microspheres," *Nat. Nanotechnol*. **3**, 413–417 (2008).
https://doi.org/10.1038/nnano.2008.150
29. J. Kim, K. Cho, I. Kim, W. M. Kim, T. S. Lee, and K.-S. Lee, "Fabrication of plasmonic nanodiscs by photonic nanojet lithography," *Appl. Phys. Express* **5**, 025201 (2012).
https://doi.org/10.1143/APEX.5.025201
30. X. A. Zhang, I.-T. Chen, and C. H. Chang, "Recent progress in near-field nanolithography using light interactions with colloidal particles: From nanospheres to three-dimensional nanostructures," *Nanotechnology* **30**, 352002 (2019).
https://doi.org/10.1088/1361-6528/ab2282
31. X. Chen, T. Wu, Z. Gong, Y. Li, Y. Zhang, and B. Li, "Subwavelength imaging and detection using adjustable and movable droplet microlenses," *Photonics Res.* **8**, 225–234 (2020).
https://doi.org/10.1364/PRJ.377795
32. V. N. Astratov, A. Darafsheh, M. D. Kerr, K. W. Allen, N. M. Fried, A. N. Antoszyk, and H. S. Ying, "Photonic nanojets for laser surgery," *SPIE Newsroom* **12**, 32–34 (2010). https://spie.org/news/2578-photonic-nanojets-for-laser-surgery?SSO=1
33. B. Yan, L. Yue, J. N. Monks, X. Yang, D. Xiong, C. Jiang, and Z. B. Wang, "Superlensing plano-convex-microsphere (PCM) lens for direct laser nano-marking and beyond," *Opt. Lett*. **45** (5), 1168–1171 (2020).
https://doi.org/10.1364/OL.380574
34. Z. Wang, W. Guo, L. Li, B. Luk'yanchuk, A. Khan, Z. Liu, Z. Chen, and M. Hong, "Optical virtual imaging at 50 nm lateral resolution with a white-light nanoscope," *Nat. Commun*. **2**, 218 (2011).
https://doi.org/10.1038/ncomms1211
35. F. Wang, L. Liu, P. Yu, Z. Liu, H. Yu, Y. Wang, and W. J. Li, "Three-dimensional super-resolution morphology by near-field assisted white-light interferometry," *Sci. Rep*. **6**, 24703 (2016).
https://doi.org/10.1038/srep24703
36. I. V. Minin and O. V. Minin, "Terahertz artificial dielectric cuboid lens on substrate for super-resolution images," *Opt. Quantum Electron*. **49**, 326 (2017).
https://doi.org/10.1007/s11082-017-1165-6
37. H. Pham, S. Hisatake, O. V. Minin, T. Nagatsuma, and I. V. Minin, "Enhancement of spatial resolution of terahertz imaging systems based on terajet generation by dielectric cube," *APL Photonics* **2** (5), 056106 (2017).
https://doi.org/10.1063/1.4983114
38. O. V. Minin, I. V. Minin, Y. Li, and J. Han, "Improvement of IR pyroelectric detector performance in THz range using wavelength-scale sphere-based terajet effect," *PIER Lett*. **101**, 29–34 (2021).
https://doi.org/10.2528/PIERL21071901
39. Y. Samura, K. Horio, V. B. Antipov, S. E. Shipilov, A. I. Eremeev, O. V. Minin, I. V. Minin, and S. Hisatake, "Characterization of mesoscopic dielectric cuboid antenna at millimeter-wave band," *IEEE Antennas Wireless Propag. Lett*. **18**, 1828–1832 (2019).
https://doi.org/10.1109/LAWP.2019.2930820
40. K. Yamada, Y. Samura, O. V. Minin, A. Kanno, N. Sekine, J. Nakajima, I. V. Minin, and S. Hisatake, "Short-range wireless transmission in the 300-GHz band using low-profile wavelength-scaled dielectric cuboid antennas," *Front. Commun. Networks* **2**, 702968 (2021).
https://doi.org/10.3389/frcmn.2021.702968
41. L. Qian and S. Jianqi, "Effect of resonant scattering on photonic jet of a microsphere," *Acta Photonica Sin*. **50**, 729002 (2021). https://www.researching.cn/ArticlePdf/m00009/2021/50/7/182.pdf
42. *Laser Cleaning*, Ed. by B. S. Luk'yanchuk (World Sci., Singapore, 2002).
https://doi.org/10.1142/4952
43. V. I. Beklemyshev, V. V. Makarov, I. I. Makhonin, Yu. N. Petrov, A. M. Prokhorov, and V. I. Pustovoy, "Photo desorption of metal ions in a semiconductor-water system," *JETP Lett*. **46** (7), 347–350 (1987).
44. W. Zapka, K. Asch, and K. Meissner, *Eur. Patent EP No.* **0297506** A2 (January 1989).
45. B. S. Luk'yanchuk, Y. W. Zheng, and Y. F. Lu, "Laser cleaning of solid surface: Optical resonance and near-field effects," *Proc. SPIE* **4065**, 576–587 (2000).
https://doi.org/10.1117/12.407350
46. H. J. Münzer, M. Mosbacher, M. Bertsch, J. Zimmermann, P. Leiderer, and J. Boneberg, "Local field enhancement effects for nanostructuring of surfaces," *J. Microsc*. **202** (1), 129–135 (2001).
https://doi.org/10.1046/j.1365-2818.2001.00876.x
47. M. Mosbacher, H.-J. Münzer, J. Zimmermann, J. Solis, J. Boneberg, and P. Leiderer, "Optical field enhancement effects in laser-assisted particle removal," *Appl. Phys. A* **72**, 41–44 (2001).
https://doi.org/10.1007/s003390000715
48. Y. F. Lu, L. Zhang, W. D. Song, Y. W. Zheng, and B. S. Luk'yanchuk, "Laser writing of a subwavelength structure on silicon (100) surfaces with particle enhanced optical irradiation," *JETP Lett*. **72** (9), 457–459 (2000).
https://doi.org/10.1134/1.1339899
49. H.-J. Münzer, M. Mosbacher, M. Bertsch, O. Dubbers, F. Burmeister, A. Pack, R. Wannemacher, B.-U. Runge, D. Bäuerle, J. Boneberg, and P. Leiderer, "Optical near-field effects in surface nanostructuring and laser cleaning," *Proc. SPIE* **4426**, 180–183 (2002).
https://doi.org/10.1117/12.456827

50. S. M. Huang, M. H. Hong, B. S. Luk'yanchuk, Y. W. Zheng, W. D. Song, Y. F. Lu, and T. C. Chong, "Pulsed laser-assisted surface structuring with optical near-field enhanced effects," *J. Appl. Phys.* **92**, 2495–2500 (2002). https://doi.org/10.1063/1.1501768

51. S. M. Huang, Z. Sun, B. S. Luk'yanchuk, M. H. Hong, and L. P. Shi, "Nanobump arrays fabricated by laser irradiation of polystyrene particle layers on silicon," *Appl. Phys. Lett.* **86**, 161911 (2005). https://doi.org/10.1063/1.1886896

52. D. Eversole, B. Luk'yanchuk, and A. Ben-Yakar, "Plasmonic laser nanoablation of silicon by the scattering of ultrafast pulses near gold nanospheres," *Appl. Phys. A* **89**, 283–291 (2007). https://doi.org/10.1007/s00339-007-4166-7

53. Z. B. Wang, W. Guo, B. S. Luk'yanchuk, A. Pena, L. Li, and Z. Liu, "Laser ablation on nanoscales," *Proc. SPIE* **7005**, S50–S61 (2008). https://doi.org/10.1117/12.780065

54. R. Fardel, E. McLeod, Y.-C. Tsai, and C. B. Arnold, "Nanoscale ablation through optically trapped microspheres," *Appl. Phys. A* **101**, 41–46 (2010). https://doi.org/10.1007/s00339-010-5792-z

55. S. M. Huang, Z. A. Wang, Z. Sun, Z. B. Wang, and B. Luk'yanchuk, "The near field properties of colloidal polystyrene microspheres on silicon," *J. Nanosci. Nanotechnol.* **11**, 10981–10985 (2011). https://doi.org/10.1166/jnn.2011.4081

56. W. J. Wang, G. H. Lim, W. D. Song, K. D. Ye, J. Zhou, M. H. Hong, and B. Liu, "Laser induced nanobump array on magnetic glass disk for low flying height application," *J. Phys.: Conf. Ser.* **59**, 177–180 (2007). https://doi.org/10.1088/1742-6596/59/1/038

57. Z. B. Wang, W. Guo, A. Pena, D. J. Whitehead, B. S. Luk'yanchuk, L. Li, Z. Liu, Y. Zhou, and M. H. Hong, "Laser micro/nano fabrication in glass with tunable-focus particle lens array," *Opt. Express* **16**, 19706–19711 (2008). https://doi.org/10.1364/OE.16.019706

58. J. F. Nye and M. V. Berry, "Dislocations in wave trains," *Proc. R. Soc. London, Ser. A* **336**, 165–190 (1974). https://doi.org/10.1098/rspa.1974.0012

59. P. Coullet, L. Gil, and F. Rocca, "Optical vortices," *Opt. Commun.* **73**, 403–408 (1989). https://doi.org/10.1016/0030-4018(89)90180-6

60. M. S. Soskin and M. V. Vasnetsov, "Singular optics," *Prog. Opt.* **42**, 219–276 (2001). https://doi.org/10.1016/S0079-6638(01)80018-4

61. M. Berry, M. Dennis, and M. Soskin, "The plurality of optical singularities," *J. Opt. A: Pure Appl. Opt.* **6**, S155–S156 (2004). https://doi.org/10.1088/1464-4258/6/5/E01

62. A. S. Desyatnikov, Y. S. Kivshar, and L. Torner, "Optical vortices and vortex solitons," *Prog. Opt.* **47**, 291–391 (2005). https://doi.org/10.1016/S0079-6638(05)47006-7

63. M. R. Dennis, K. O'Holleran, and M. J. Padgett, "Singular optics: Optical vortices and polarization singularities," *Prog. Opt.* **53**, 293–363 (2009). https://doi.org/10.1016/S0079-6638(08)00205-9

64. M. R. Dennis, Y. S. Kivshar, M. S. Soskin, and G. A. Swartzlander, Jr., "Singular optics: More ado about nothing," *J. Opt. A: Pure Appl. Opt.* **11**, 090201 (2009). https://doi.org/10.1088/1464-4258/11/9/090201

65. L. Allen, M. W. Beijersbergen, R. J. C. Spreeuw, and J. P. Woerdman, "Orbital angular momentum of light and the transformation of Laguerre–Gaussian laser modes," *Phys, Rev. A* **45**, 8185–8189 (1992). https://doi.org/10.1103/PhysRevA.45.8185

66. X. Cai, J. Wang, M. J. Strain, B. Johnson-Morris, J. B. Zhu, M. Sorel, J. L. O'Brien, M. G. Thompson, and S. Yu, "Integrated compact optical vortex beam emitters," *Science* **338**, 363–366 (2012). https://doi.org/10.1364/AO.384838

67. Z. B. Wang, B. S. Luk'yanchuk, M. H. Hong, Y. Lin, and T. C. Chong, "Energy flows around a small particle investigated by classical Mie theory," *Phys. Rev. B* **70**, 035418 (2004). https://doi.org/10.1103/PhysRevB.70.035418

68. M. V. Bashevoy, V. A. Fedotov and N. I. Zheludev, "Optical whirlpool on an absorbing metallic nanoparticle," *Opt. Express* **13**, 8372–8379 (2005). https://doi.org/10.1364/OPEX.13.008372

69. B. S. Luk'yanchuk and V. Ternovsky, "Light scattering by thin wire with surface plasmon resonance: Bifurcations of the Poynting vector field," *Phys. Rev. B* **73**, 235432 (2006). https://doi.org/10.1103/PhysRevB.73.235432

70. B. S. Luk'yanchuk, M. I. Tribelsky, and V. Ternovsky, "Light scattering at nanoparticles close to plasmon resonance frequencies," *J. Opt. Technol.* **73** (6), 371–377 (2006). https://doi.org/10.1364/JOT.73.000371

71. B. S. Luk'yanchuk, Z. B. Wang, M. Tribelsky, V. Ternovsky, M. H. Hong, and T. C. Chong, "Peculiarities of light scattering by nanoparticles and nanowires near plasmon resonance frequencies," *J. Phys.: Conf. Ser.* **59**, 234–239 (2007). https://doi.org/10.1088/1742-6596/59/1/050

72. B. S. Luk'yanchuk, M. I. Tribelsky, V. Ternovsky, Z. B. Wang, M. H. Hong, L. P. Shi, and T. C. Chong, "Peculiarities of light scattering by nanoparticles and nanowires near plasmon resonance frequencies in weakly dissipating materials," *J. Opt. A: Pure Appl. Opt.* **9**, S294–S300 (2007). https://doi.org/10.1088/1464-4258/9/9/S03

73. I. V. Minin, O. V. Minin, Y. Cao, B. Yan, Z. B. Wang, and B. Luk'yanchuk, "Photonic lenses with whispering gallery waves at Janus particles," *Opto-Electron. Sci.* **1** (2), 210008 (2022). https://doi.org/10.29026/oes.2022.210008

74. E. D. Palik, *Handbook of Optical Constants of Solids* (Academic, New York, 1985). https://www.elsevier.com/books/handbook-of-optical-constants-of-solids/palik/978-0-08-055630-7

75. M. Kerker, D.-S. Wang, and C. L. Giles, "Electromagnetic scattering by magnetic spheres," *J. Opt. Soc. Am.* **73** (6), 765–767 (1983). https://doi.org/10.1364/JOSA.73.000765

76. B. García-Cámara, J. M. Saiz, F. González, and F. Moreno, "Nanoparticles with unconventional scat-

tering properties: Size effects," *Opt. Commun.* **283**, 490–496 (2010). https://doi.org/10.1016/j.optcom.2009.10.027

77. W. Liu and Y. S. Kivshar, "Generalized Kerker effects in nanophotonics and meta-optics [Invited]," *Opt Express* **26**, 13085–13105 (2018). https://doi.org/10.1364/OE.26.013085
78. Z. B. Wang, B. Luk'yanchuk, L. Yue, B. Yan, J. Monks, R. Dhama, O. V. Minin, I. V. Minin, S. M. Huang, and A. A. Fedyanin, "High order Fano resonances and giant magnetic fields in dielectric microspheres," *Sci. Rep.* **9**, 20293 (2019). https://doi.org/10.1038/s41598-019-56783-3
79. A. B. Evlyukhin, C. Reinhardt, A. Seidel, B. Luk'yanchuk, and B. N. Chichkov, "Optical response features of Si-nanoparticle arrays," *Phys. Rev. B* **82**, 045404 (2010). https://doi.org/10.1103/PhysRevB.82.045404
80. A. García-Etxarri, R. Gómez-Medina, L. S. Froufe-Pérez, C. López, L. Chantada, F. Scheffold, J. Aizpurua, M. Nieto-Vesperinas, and J. J. Sáenz, "Strong magnetic response of submicron silicon particles in the infrared," *Opt. Express* **19**, 4815–4826 (2011). https://doi.org/10.1364/OE.19.004815
81. A. I. Kuznetsov, A. E. Miroshnichenko, Y. H. Fu, J. B. Zhang, and B. Luk'yanchuk, "Magnetic light," *Sci. Rep.* **2**, 492 (2012). https://doi.org/10.1038/srep00492
82. A. B. Evlyukhin, S. M. Novikov, U. Zywietz, R. L. Eriksen, C. Reinhardt, S. I. Bozhevolnyi, and B. N. Chichkov, "Demonstration of magnetic dipole resonances of dielectric nanospheres in the visible region," *Nano Lett.* **12**, 3749–3755 (2012). https://doi.org/10.1021/nl301594s
83. J. M. Geffrin, B. García-Cámara, R. Gómez-Medina, P. Albella, L. S. Froufe-Pérez, C. Eyraud, A. Litman, R. Vaillon, F. González, M. Nieto-Vesperinas, and J. J. Sáenz, "Magnetic and electric coherence in forward-and back-scattered electromagnetic waves by a single dielectric subwavelength sphere," *Nat. Commun.* **3**, 1171 (2012). https://doi.org/10.1038/ncomms2167
84. Y. H. Fu, A. I. Kuznetsov, A. E. Miroshnichenko, Y. F. Yu, and B. Luk'yanchuk, "Directional visible light scattering by silicon nanoparticles," *Nat. Commun.* **4**, 1527 (2013). https://doi.org/10.1038/ncomms2538
85. S. Person, M. Jain, Z. Lapin, J. J. Sáenz, G. Wicks, and L. Novotny, "Demonstration of zero optical backscattering from single nanoparticles," *Nano Lett.* **13**, 1806–1809 (2013). https://doi.org/10.1021/nl4005018
86. R. Paniagua-Domingues, B. Luk'yanchuk, and A. I. Kuznetsov, "Control of scattering by isolated dielectric nanoantennas," in *Dielectric Metamaterials: Fundamentals Designs and Applications* (Elsevier, Netherlands, 2020), Chap. 3, pp. 73–108. https://doi.org/10.1016/B978-0-08-102403-4.00008-6
87. B. Luk'yanchuk, N. Voshchinnikov, R. Paniagua-Dominguez, and A. Kuznetsov, "Optimum forward light scattering by spherical and spheroidal dielectric nanoparticles with high refractive index," *ACS Photonics* **2**, 993–999 (2015). https://doi.org/10.1021/acsphotonics.5b00261
88. H. K. Shamkhi, K. V. Baryshnikova, A. Sayanskiy, P. Kapitanova, P. D. Terekhov, P. Belov, A. Karabchevsky, A. B. Evlyukhin, Y. Kivshar, and A. S. Snalin, "Transverse scattering and generalized Kerker effects in all-dielectric Mie-resonant metaoptics," *Phys. Rev. Lett.* **122**, 193905 (2019). https://doi.org/10.1103/PhysRevLett.122.193905
89. V. Savinov, N. Papasimakis, D. P. Tsai, and N. I. Zheludev, "Optical anapoles," *Commun. Phys.* **2**, 1–4 (2019). https://doi.org/10.1038/s42005-019-0167-z
90. B. Luk'yanchuk, N. I. Zheludev, S. A. Maier, N. J. Halas, P. Nordlander, H. Giessen, and T. C. Chong, "The Fano resonance in plasmonic nanostructures and metamaterials," *Nat. Mater.* **9**, 707–715 (2010). https://doi.org/10.1038/nmat2810
91. A. E. Miroshnichenko, S. Flach, and Y. S. Kivshar, "Fano resonances in nanoscale structures," *Rev. Mod. Phys.* **82**, 2257–2298 (2010). https://doi.org/10.1103/RevModPhys.82.2257
92. A. I. Musorin, M. G. Barsukova, A. S. Shorokhov, B. S. Luk'yanchuk, and A. A. Fedyanin, "Manipulating light intensity by mangetophotonic metasurfaces," *J. Magn. Magn. Mater.* **459**, 165 (2018). https://doi.org/10.1016/j.jmmm.2017.11.049
93. M. G. Barsukova, A. I. Musorin, A. S. Shorokhov, and A. A. Fedyanin, "Enhanced magneto-optical effects in hybrid Ni–Si metasurfaces," *APL Photonics* **4**, 016102 (2019). https://doi.org/10.1063/1.5066307
94. F. Hao, P. Nordlander, Y. Sonnefraud, P. Van Dorpe, and S. A. Maier, "Tunability of subradiant dipolar and Fano type plasmon resonances in metallic ring/disk cavities: Implications for nanoscale optical sensing," *ACS Nano* **3**, 643–652 (2009). https://doi.org/10.1021/nn900012r
95. Y. Sonnefraud, N. Verellen, H. Sobhani, G. A. E. Vandenbosch, V. V. Moshchalkov, P. Van Dorpe, P. Nordlander, and S. A. Maier, "Experimental realization of subradiant, superradiant, and Fano resonances in ring/disk plasmonic nanocavities," *ACS Nano* **4**, 1664–1670 (2010). https://doi.org/10.1021/nn901580r
96. D. Dregely, M. Hentschel, and H. Giessen, "Excitation and tuning of higher-order Fano resonances in plasmonic oligomer clusters," *ACS Nano* **5**, 8202–8211 (2011). https://doi.org/10.1021/nn202876k
97. Y. H. Fu, J. B. Zhang, Y. F. Yu, and B. Luk'yanchuk, "Generating and manipulating higher order Fano resonances in dual-disk ring plasmonic nanostructures," *ACS Nano* **6**, 5130–5137 (2012). https://doi.org/10.1021/nn3007898
98. C. L. Garrido Alzar, M. A. G. Martinez, and P. Nussenzveig, "Classical analog of electromagnetically induced transparency," *Am. J. Phys.* **70** (1), 37–41 (2002). https://doi.org/10.1119/1.1412644
99. Y. S. Joe, A. M. Satanin, and C. S. Kim, "Classical analogy of Fano resonances," *Phys. Scr.* **74** (2), 259–266 (2006). https://doi.org/10.1088/0031-8949/74/2/020

100. M. I. Rabinovich and D. I. Trubetskov, *Oscillations and Waves in Linear and Nonlinear Systems* (Kluwer Academic, Dordrecht, 1989). https://doi.org/10.1017/S0022112091221278

101. N. Papasimakis and N. I. Zheludev, "Metamaterial-induced transparency: Sharp Fano resonances and slow light," *Opt. Photonics News* **20** (10), 22–27 (2009). https://doi.org/10.1364/OPN.20.10.000022

102. M. Rahmani, B. Lukiyanchuk, and M. H. Hong, "Fano resonance in novel plasmonic nanostructures," *Laser Photonics Rev*. **7**, 329–349 (2013). https://doi.org/10.1002/lpor.201200021

103. B. S. Luk'yanchuk, Z. B. Wang, A. E. Miroshnichenko, Yu. S. Kivshar, A. I. Kuznetsov, D. L. Gao, L. Gao, and C.-W. Qiu, "Nano-Fano resonances and topological optics," in *Singular and Chiral Nanoplasmonics*, Ed. by S. Boriskina and N. I. Zheludev (CRC Press, Boca Raton, FL, 2014), Chap. 9, pp. 285–310. ISBN 9789814613170.

104. M. I. Tribelsky and A. E. Miroshnichenko, "Giant in-particle field concentration and Fano resonances at light scattering by high-refractive-index particles," *Phys. Rev. A* **93**, 053837 (2016). https://doi.org/10.1103/PhysRevA.93.053837

105. L. Yue, Z. Wang, B. Yan, J. Monks, Y. Joya, R. Dhama, O. V. Minin, and I. V. Minin, "Super-enhancement focusing of teflon spheres," *Ann. Phys*. **532**, 2000373 (2020). https://doi.org/10.1002/andp.202000373

106. B. Luk'yanchuk, L. M. Vasilyak, V. Ya. Pecherkin, S. P. Vetchinin, V. E. Fortov, Z. B. Wang, R. Paniagua-Domínguez, and A. A. Fedyanin, "Colossal magnetic fields in high refractive index materials at microwave frequencies," *Sci. Rep*. **11**, 23453 (2021). https://doi.org/10.1038/s41598-021-01644-1

107. B. S. Luk'yanchuk, A. E. Miroshnichenko, and Y. S. Kivshar, "Fano resonances and topological optics: An interplay of far- and near-field interference phenomena," *J. Opt.* **15**, 073001 (2013). https://doi.org/10.1088/2040-8978/15/7/073001

108. Y. Aharonov, F. Colombo, I. R. Sabadini, D. C. Struppa, and J. Tollaksen, "Some mathematical properties of superoscillations," *J. Phys. A: Math. Theor*. **44**, 365304 (2011). https://doi.org/10.1088/1751-8113/44/36/365304

109. M. V. Berry and N. Moiseyev, "Superoscillations and supershifts in phase space: Wigner and Husimi function interpretations," *J. Phys. A: Math. Theor*. **47**, 315203 (2014). https://doi.org/10.1088/1751-8113/47/31/315203

110. M. Berry, N. Zheludev, Y. Aharonov, F. Colombo, I. Sabadini, D. C. Struppa, J. Tollaksen, E. T. Rogers, F. Qin, M. Hong, and X. Luo, "Roadmap on superoscillations," *J. Opt*. **21**, 053002 (2019). https://doi.org/10.1088/2040-8986/ab0191

111. M. V. Berry and S. Popescu, "Evolution of quantum superoscillations and optical superresolution without evanescent waves," *J. Phys. A: Math. Gen*. **39**, 6965 (2006). https://doi.org/10.1088/0305-4470/39/22/011

112. N. I. Zheludev, "What diffraction limit?" *Nat. Mater*. **7**, 420–422 (2008). https://doi.org/10.1038/nmat2163

113. M. V. Berry, "Five momenta," *Eur. J. Phys*. **44**, 1337–1348 (2003). https://doi.org/10.1088/0143-0807/34/6/1337

114. B. S. Luk'yanchuk, T. C. Chong, L. P. Shi, M. I. Tribelsky, Z. B. Wang, L. Li, C. W. Qiu, C. J. R. Sheppard, and J. H. Wu, "What we expect from weakly dissipating materials at the range of plasmon resonance frequencies," *IEEE PhotonicsGlobal@Singapore* (*IPGS*), *Singapore, December 8–11, 2008* (IEEE, 2009), Vols. 1–2, pp. 187–190. https://doi.org/10.1109/IPGC.2008.4781348

115. V. B. Gil'denburg and I. G. Kondrat'ev, "Diffraction of electromagnetic waves by a bounded plasma in the presence of spatial dispersion," *Radiotekh. Electron*. **10**, 658–664 (1965) [in Russian].

116. M. I. Tribel'skii, "Resonant scattering of light by small particles," *Zh. Eksp. Teor. Fiz*. **86**, 915–919 (1984) [in Russian].

117. M. I. Tribelsky and B. S. Luk'yanchuk, "Anomalous light scattering by small particles," *Phys. Rev. Lett*. **97**, 263902 (2006). https://doi.org/10.1103/PhysRevLett.97.263902

118. M. I. Tribelsky and B. S. Luk'yanchuk, "Light scattering by small particles and their light heating: New aspects of the old problems," in *Fundamentals of Laser-Assisted Micro- and Nanotechnologies* (Springer, Cham, 2014), Chap. 6, pp. 125–146. https://doi.org/10.1007/978-3-319-05987-7_6

119. L. D. Landau and E. M. Lifshitz, *Electrodynamics of Continuous Media* (Butterworth-Heinemann, Oxford, 2002). ISBN 9780750626347.

120. M. I. Tribelsky, "Anomalous light absorption by small particles," *Europhys. Lett*. **94**, 14004 (2011). https://doi.org/10.1209/0295-5075/94/14004

121. B. S. Luk'yanchuk, A. E. Miroshnichenko, M. I. Tribelsky, Y. S. Kivshar, and A. R. Khokhlov, "Paradoxes in laser heating of plasmonic nanoparticles," *New J. Phys*. **14**, 093022 (2012). https://doi.org/10.1088/1367/1-26304/9/093022

122. C. F. Bohren, "How can a particle absorb more than the light incident on it?" *Am. J. Phys*. **51**, 323–327 (1983). https://doi.org/10.1119/1.13262

123. B. Klębowski, J. Depciuch, M. Parlińska-Wojtan, and J. Baran, "Applications of noble metal-based nanoparticles in medicine," *Int. J. Mol. Sci*. **19**, 4031 (2018). https://doi.org/10.3390/ijms19124031

124. N. Papasimakis, V. A. Fedotov, V. Savinov, T. A. Raybould, and N. I. Zheludev, "Electromagnetic toroidal excitations in matter and free space," *Nat. Mater*. **15**, 263–271 (2016). https://doi.org/10.1038/nmat4563

125. G. N. Afanasiev and V. M. Dubovik, "Some remarkable charge-current configurations," *Phys. Part. Nucl*. **29** (4), 366–391 (1998). https://wwwinfo.jinr.ru/publish/Archive/Pepan/1998-v29/v-29-4/pdf_obzory/v29p4_03.pdf

126. Ya. B. Zeldovich, "Electromagnetic interaction with parity violation," *Sov. Phys.-JETP* **6**, 1184–1186 (1958).

127. E. E. Radescu and G. Vaman, "Exact calculation of the angular momentum loss, recoil force, and radiation intensity for an arbitrary source in terms of electric, magnetic, and toroid multipoles," *Phys. Rev. E* **65**, 046609 (2002). https://doi.org/10.1103/PhysRevE.65.046609

128. C. M. Ho and R. J. Scherrer, "Anapole dark matter," *Phys. Lett. B* **722**, 341–346 (2013). https://doi.org/10.1016/j.physletb.2013.04.039

129. A. E. Miroshnichenko, A. B. Evlyukhin, Y. F. Yu, R. M. Bakker, A. Chipouline, A. I. Kuznetsov, B. Luk'yanchuk, B. N. Chichkov, and Y. S. Kivshar, "Nonradiating anapole modes in dielectric nanoparticles," *Nat. Commun*. **6**, 8069 (2015). https://doi.org/10.1038/ncomms9069

130. B. Luk'yanchuk, R. Paniagua-Domínguez, A. I. Kuznetsov, A. E. Miroshnichenko, and Y.S. Kivshar, "Suppression of scattering for small dielectric particles: Anapole mode and invisibility," *Philos. Trans. R. Soc., A* **375**, 20160069 (2017). https://doi.org/ https://doi.org/10.1098/rsta.2016.0069

131. B. Luk'yanchuk, R. Paniagua-Domínguez, A. I. Kuznetsov, A. E. Miroshnichenko, and Y. S. Kivshar, "Hybrid anapole modes of high-index dielectric nanoparticles," *Phys. Rev. A* **95**, 063820 (2017). https://doi.org/10.1103/PhysRevA.95.063820

132. T. Kaelberer, V. A. Fedotov, N. Papasimakis, D. P. Tsai, and N. I. Zheludev, "Toroidal dipolar response in a metamaterial," *Science* **330**, 1510–1512 (2010). https://doi.org/10.1126/science.1197172

133. B. Ögüt, N. Talebi, R. Vogelgesang, W. Sigle, and P. A. van Aken, "Toroidal plasmonic eigenmodes in oligomer nanocavities for the visible," *Nano Lett*. **12** (10), 5239–5244 (2012). https://doi.org/10.1021/nl302418n

134. A. A. Basharin, M. Kafesaki, E. N. Economou, C. M. Soukoulis, V. A. Fedotov, V. Savinov, and N. I. Zheludev, "Dielectric metamaterials with toroidal dipolar response," *Phys. Rev. X* **5**, 011036 (2015). https://doi.org/10.1103/PhysRevX.5.011036

135. L. Wei, Z. Xi, N. Bhattacharya, and H. P. Urbach, "Excitation of the radiationless anapole mode," *Optica* **3**, 799–802 (2016). https://doi.org/10.1364/OPTICA.3.000799

136. A. A. Basharin, V. Chuguevsky, N. Volsky, M. Kafesaki, and E. N. Economou, "Extremely high Q-factor metamaterials due to anapole excitation," *Phys. Rev. B* **95**, 035104 (2017). https://doi.org/10.1103/PhysRevB.95.035104

137. J. S. T. Gongora, A. E. Miroshnichenko, Y. S. Kivshar, and A. Fratalocchi, "Anapole nanolasers for mode-locking and ultrafast pulse generation," *Nat. Commun*. **8**, 15535 (2017). https://doi.org/10.1038/ncomms15535

138. P. C. Wu, C. Y. Liao, V. Savinov, T. L. Chung, W. T. Chen, Y. W. Huang, P. R. Wu, Y. H. Chen, A. Q. Liu, N. I. Zheludev, and D. P. Tsai, "Optical anapole metamaterial," *ACS Nano* **12**, 1920–1927 (2018). https://doi.org/10.1021/acsnano.7b08828

139. K. V. Baryshnikova, D. A. Smirnova, B. S. Luk'yanchuk, and Y. S. Kivshar, "Optical anapoles: Concepts and applications," *Adv. Opt. Mater*. **7**, 1801350 (2019). https://doi.org/10.1002/adom.201801350

140. N. Pavlov, I. Stenishchev, A. Ospanova, P. Belov, P. Kapitanova, and A. Basharin, "Toroidal dipole mode observation in situ," *Phys. Status Solidi B* **257**, 1900406 (2020). https://doi.org/10.1002/pssb.201900406

141. K. E. Ballantine and J. Ruostekoski, "Radiative toroidal dipole and anapole excitations in collectively responding arrays of atoms," *arXiv:2005.05918v1* (2020)

142. D. C. Zografopoulos, A. Ferraro, J. F. Algorri, P. Martín-Mateos, B. García-Cámara, A. Moreno-Oyervides, V. Krozer, P. Acedo, R. Vergaz, J. M. Sánchez-Pena, and R. Beccherelli, "All-dielectric silicon metasurface with strong subterahertz toroidal dipole resonance," *Adv. Opt. Mater*. **7** (19), 1900777 (2019). https://doi.org/10.1002/adom.201900777

143. D. C. Zografopoulos, J. F. Algorri, A. Ferraro, B. García-Cámara, J. M. Sánchez-Pena, and R. Beccherelli, "Toroidal metasurface resonances in microwave waveguides," *Sci. Rep*. **9**, 7544 (2019). https://doi.org/10.1038/s41598-019-44093-7

144. A. K. Ospanova, I. V. Stenishchev, and A. A. Basharin, "Anapole mode sustaining silicon metamaterials in visible spectral range," *Laser Photonics Rev*. **12**, 1870031 (2018). https://doi.org/10.1002/lpor.201870031

145. J. F. Algorri, D. C. Zografopoulos, A. Ferraro, B. García-Cámara, R. Vergaz, R. Beccherelli, and J. M. Sánchez-Pena, "Anapole modes in hollow nanocuboid dielectric metasurfaces for refractometric sensing," *Nanomaterials* **9**, 30 (2018). https://doi.org/10.3390/nano9010030

146. N. A. Nemkov, A. A. Basharin, and V. A. Fedotov, "Nonradiating sources, dynamic anapole, and Aharonov–Bohm effect," *Phys. Rev. B* **95**, 165134 (2017). https://doi.org/10.1103/PhysRevB.95.165134

147. N. A. Nemkov, I. V. Stenishchev, and A. A. Basharin, "Nontrivial nonradiating all-dielectric anapole," *Sci. Rep*. **7**, 1064 (2017). https://doi.org/10.1038/s41598-017-01127-2

148. V. A. Zenin, C. E. Garcia-Ortiz, A. B. Evlyukhin, Y. Yang, R. Malureanu, S. M. Novikov, V. Coello, B. N. Chichkov, S. I. Bozhevolnyi, A. V. Lavrinenko, and N. A. Mortensen, "Engineering nanoparticles with pure high-order multipole scattering," *ACS Photonics* **7**, 1067–1075 (2020). https://doi.org/10.1021/acsphotonics.0c00078

149. M. Gupta, Y. K. Srivastava, and R. Singh, "A toroidal metamaterial switch," *Adv. Mater*. **30**, 1704845 (2018). https://doi.org/10.1002/adma.201704845

150. L. Cong, V. Savinov, Y. K. Srivastava, S. Han, and R. Singh, "A metamaterial analog of the Ising model," *Adv. Mater*. **30**, 1804210 (2018). https://doi.org/10.1002/adma.201804210

151. M. Gupta and R. Singh, "Toroidal versus Fano resonances in high Q planar THz metamaterials," *Adv. Opt.*

Mater. **4**, 2119–2125 (2016). https://doi.org/10.1002/adom.201600553

152. M. Gupta, V. Savinov, N. Xu, L. Cong, G. Dayal, S. Wang, W. Zhang, N. I. Zheludev, and R. Singh, "Sharp toroidal resonances in planar terahertz metasurfaces," *Adv. Mater.* **28**, 8206–8211 (2016). https://doi.org/10.1002/adma.201601611
153. A. K. Ospanova, A. Basharin, A. E. Miroshnichenko, and B. Luk'yanchuk, "Generalized hybrid anapole modes in all-dielectric ellipsoid particles [Invited]," *Opt. Mater. Express* **11**, 23–34 (2021). https://doi.org/10.1364/OME.414340
154. Y. Yang, V. A. Zenin, and S. I. Bozhevolnyi, "Anapole-assisted strong field enhancement in individual all-dielectric nanostructures," *ACS Photonics* **5**, 1960–1966 (2018). https://doi.org/10.1021/acsphotonics.7b01440
155. G. Grinblat, Y. Li, M. P. Nielsen, R. F. Oulton, and S. A. Maier, "Enhanced third harmonic generation in single germanium nanodisks excited at the anapole mode," *Nano Lett.* **16**, 4635 (2016). https://doi.org/10.1021/acs.nanolett.6b01958
156. G. Grinblat, Y. Li, M. P. Nielsen, R. F. Oulton, and S. A. Maier, "Efficient third harmonic generation and nonlinear subwavelength imaging at a higher-order anapole mode in a single germanium nanodisk," *ACS Nano* **11**, 953–960 (2016). https://doi.org/10.1021/acsnano.6b07568
157. T. Shibanuma, G. Grinblat, P. Albella, and S. A. Maier, "Efficient third harmonic generation from metal–dielectric hybrid nanoantennas," *Nano Lett.* **17**, 2647–2651 (2017). https://doi.org/10.1021/acs.nanolett.7b00462
158. V. F. Gili, L. Ghirardini, D. Rocco, G. Marino, I. Favero, I. Roland, G. Pellegrini, L. Duò, M. Finazzi, L. Carletti, A. Locatelli, A. Lemaître, D. Neshev, C. De Angelis, G. Leo, and M. Celebrano, "Metal–dielectric hybrid nanoantennas for efficient frequency conversion at the anapole mode," *Beilstein J. Nanotechnol.* **9**, 2306–2314 (2018). https://doi.org/10.3762/bjnano.9.215
159. K. Koshelev, G. Favraud, A. Bogdanov, Y. Kivshar, and A. Fratalocchi, "Nonradiating photonics with resonant dielectric nanostructures," *Nanophotonics* **8**, 725–745 (2019). https://doi.org/10.1515/nanoph-2019-0024
160. M. Timofeeva, L. Lang, F. Timpu, C. Renaut, A. Bouravleuv, I. Shtrom, G. Cirlin, and R. Grange, "Anapoles in free-standing III–V nanodisks enhancing second-harmonic generation," *Nano Lett.* **18**, 3695–3702 (2018). https://doi.org/10.1021/acs.nanolett.8b00830
161. L. Xu, M. Rahmani, K. Z. Kamali, A. Lamprianidis, L. Ghirardini, J. Sautter, R. Camacho-Morales, H. Chen, M. Parry, I. Staude, G. Zhang, D. Neshev, and A. E. Miroshnichenko, "Boosting third-harmonic generation by a mirror-enhanced anapole resonator," *Light: Sci. Appl.* **7**, 44 (2018). https://doi.org/10.1038/s41377-018-0051-8
162. A. V. Panov, "Optical Kerr nonlinearity of arrays of all-dielectric high-index nanodisks in the vicinity of the anapole state," *Opt. Lett.* **45**, 3071–3074 (2020). https://doi.org/10.1364/OL.391991
163. J. Yao, B. Li, G. Cai, and Q. H. Liu, "Doubly mirror-induced electric and magnetic anapole modes in metal-dielectric-metal nanoresonators," *Opt. Lett.* **46**, 576–579 (2021). https://doi.org/10.1364/OL.415423
164. A. Tripathi, H. R. Kim, P. Tonkaev, S. J. Lee, S. V. Makarov, S. S. Kruk, M. V. Rybin, H. G. Park, and Y. Kivshar, "Lasing action from anapole metasurfaces," *Nano Lett.* **21**, 6563–6568 (2021). https://doi.org/10.1021/acs.nanolett.1c01857
165. M. V. Rybin, K. L. Koshelev, Z. F. Sadrieva, K. B. Samusev, A. A. Bogdanov, M. F. Limonov, and Y. S. Kivshar, "High-Q supercavity modes in subwavelength dielectric resonators," *Phys. Rev. Lett.* **119**, 243901 (2017). https://doi.org/10.1103/PhysRevLett.119.243901
166. J. von Neumann and E. Wigner, "Über merkwürdige diskrete Eigenwerte," *Phys. Z.* **30**, 465–467 (1929)," in *Collected Works of Eugene Paul Wigner* (Springer, 1993), pp. 291–293. https://ui.adsabs.harvard.edu/abs/1929PhyZ...30..467V/abstract
167. H. Friedrich and D. Wintgen, "Interfering resonances and bound states in the continuum," *Phys. Rev. A* **32**, 3231–3242 (1985). https://doi.org/10.1103/PhysRevA.32.3231
168. C. W. Hsu, B. Zhen, A. D. Stone, J. D. Joannopoulos, and M. Soljačić, "Bound states in the continuum," *Nat. Rev. Mater.* **1**, 16048 (2016). https://doi.org/10.1038/natrevmats.2016.48
169. K. Koshelev, A. Bogdanov, and Yu. Kivshar, "Engineering with bound states in the continuum," *Opt. Photonics News* **31**, 38–45 (2020). https://doi.org/10.1364/OPN.31.1.000038
170. S. T. Ha, Y. H. Fu, N. K. Emani, Z. Pan, R. M. Bakker, R. Paniagua-Domínguez, and A. I. Kuznetsov, "Directional lasing in resonant semiconductor nanoantenna arrays," *Nat. Nanotechnol.* **13**, 1042–1047 (2018). https://doi.org/10.1038/s41565-018-0245-5
171. A. M. Chernyak, M. G. Barsukova, A. S. Shorokhov, A. I. Musorin, and A. A. Fedyanin, "Bound states in the continuum in magnetophotonic metasurfaces," *JETP Lett.* **111**, 46–49 (2020). https://doi.org/10.1134/S0021364020010105
172. O. V. Minin and I. V. Minin, "Optical phenomena in mesoscale dielectric particles," *Photonics* **8**, 591 (2021). https://doi.org/10.3390/photonics8120591

Translated by Yu. Sin'kov

SPELL: 1. ok